Late Quaternary faulting in southern Matese (central Italy): implications for earthquake potential in the southern Apennines

Paolo Boncio[1,2], Eugenio Auciello[3], Vincenzo Amato[4], Pietro Aucelli[5], Paola Petrosino[6], Anna C. Tangari[1], Brian R. Jicha[7]

[1]Department DiSPUTer, Università degli Studi G. d'Annunzio Chieti - Pescara, Chieti, 66100, Italy
[2]CRUST – Interuniversity Center for 3D Seismotectonics with territorial Applications, Chieti, 66100, Italy
[3]Geoscience practitioner, Pesche (IS), Italy
[4]Department of Biosciences and Territory, Università degli Studi del Molise, Pesche (IS), 86090, Italy
[5]Department of Science and Technology, Università degli Studi di Napoli Parthenope, Neaples, 80133, Italy
[6]Università degli Studi di Napoli Federico II, Department of Earth, Environmental and Resources Sciences, Neaples, 80126, Italy
[7]University of Wisconsin-Madison, Department of Geoscience, Madison, Wisconsin 53706-1692, USA

Correspondence to: Paolo Boncio (paolo.boncio@unich.it)

Abstract. We studied in detail the Gioia Sannitica active normal fault (GF) along the Southern Matese Fault system in the southern Apennines of Italy. The current activity of the fault system and its potential to produce strong earthquakes have been underestimated so far, and are now defined. Precise mapping of the GF fault trace on a 1:20,000 geological map and several point data on geometry, kinematics and throw rate are made available in electronic format. The GF, and in general the entire fault system along the southern Matese mountain front, is made of slowly-slipping faults, with a long active history revealed by the large geologic offsets, mature geomorphology, and complex fault pattern and kinematics. Present activity has resulted in Late Quaternary fault scarps resurrecting the foot of the mountain front, and Holocene surface faulting. The slip rate varies along-strike, with maximum Late Pleistocene – Holocene throw rate of ~0.5 mm/yr. Activation of the 11.5 km-long GF can produce up to M 6.1 earthquakes. If activated together with the 18 km-long Ailano-Piedimonte Matese fault (APMF), the seismogenic potential would be M 6.8. The slip history of the two faults is compatible with a contemporaneous rupture. The observed Holocene displacements on the GF and APMF are compatible with activations during some poorly known historical earthquakes, such as the 1293 (M 5.8), 1349 (M 6.8; southern prolongation of the rupture on the Aquae Iuliae fault?) and CE 346 earthquakes. A fault rupture during the 847 poorly-constrained historical earthquake is also compatible with the dated displacements.

1 Introduction

Detailed field mapping of active faulting is essential for populating fault databases oriented at mitigating the seismic risk from ground shaking and fault displacement hazard (e.g., DISS Working Group, 2018; Styron and Pagani, 2020; Faure Walker et al., 2021; California U.S. Alquist-Priolo Earthquake Fault Zoning Act, https://www.conservation.ca.gov/cgs/alquist-priolo; New Zealand Active Faults Database, https://data.gns.cri.nz/af/; ITaly HAzards from CApable faults, ITHACA,

http://sgi2.isprambiente.it/ithacaweb/). The implementation of accurate fault mapping is particularly important in areas where geodetic or seismologic evidence of active tectonics contrast with poor knowledge of active faulting from surface geology.

35 In the central-southern Apennines of Italy, presently stretching at rates of ~3 mm/yr in the SW-NE direction, two areas were highlighted as being characterized by significant deficit of seismic moment release for the last 500 years (D'Agostino, 2014; Fig. 1). Shortly after the characterization, one of the areas was struck by the 2016 central Italy normal faulting earthquakes on the Mt. Vettore – Mt. Bove normal fault (maximum Mw = 6.5; Chiaraluce et al., 2017; Civico et al., 2018). The second area extends for ~80 km between the central and southern Apennines, and includes a large part of the Matese Mts. In the Mt. Vettore 40 – Mt. Bove area, paleoseismologic studies have demonstrated that the fault responsible for the 2016 earthquake ruptured repeatedly in prehistoric times, with average recurrence interval 1.8±0.3 kyr, and the penultimate earthquake occurred well before the historical catalogue (Cinti et al., 2019; Galli et al. 2019). Thus, the 2016 earthquakes demonstrate that the geology of active faults is equally as critical as historical seismicity for estimating the true seismic potential in areas characterized by low strain rates (velocities of a few mm/yr) and long return periods of strong earthquakes ($\geq$ M 6.5), such as the Italian 45 Apennines. This has implications in seismic hazard assessments (e.g., Valentini et al., 2019).

In the Matese Mts, the geology of active faults is poorly constrained, with only two known active normal faults: the SW-dipping Aquae Iuliae fault and the NE-dipping Northern Matese fault system (Di Bucci et al., 2005; Galli and Naso, 2009; Boncio et al., 2016; Ferrarini et al., 2017; Galli et al., 2017) (Fig. 1). To the SE, the activity of the Matese normal faults is less constrained. In a recent attempt to derive fault slip rates from geodetic data for the Matese area (Carafa et al., 2020), the results 50 were not conclusive due to the sparseness of GNSS stations and the paucity of geologic constraints.

This paper focuses on the normal faults cropping out along the southern slopes of the Matese Mts., named Southern Matese Fault system (Ailano – Piedimonte Matese and Gioia Sannitica faults). We describe in detail the geology of the Gioia Sannitica normal fault, in the southern part of the system (a detailed, 1:20,000 geologic map is attached as supplementary material; Plate S1). For the first time, we show clear evidence of late Quaternary and Holocene faulting, thanks to detailed field analyses of 55 fault zones in Quaternary sediments and dating (^{14}C and ^{40}Ar/^{39}Ar) of faulted sediments. The data and observations of active faulting along the Gioia Sannitica normal fault are combined with new and pre-existing data from the northern part of the system and discussed together in terms of overall seismogenic potential of the Southern Matese Fault system.

2 Geologic and seismotectonic setting

2.1 General geologic setting

60 The Matese Mts. form a 20 km-wide, 50 km-long massif of carbonate rocks elongated in the NW-SE direction, in the northern part of the southern Apennines of Italy. The massif has a maximum elevation of about 2000 m a.s.l. and is delimited to the NE by the Bojano depression and to the W and SW by the valley of the Voltuno River (Venafro and Alife depressions). This morphologic setting is largely due to Quaternary extensional tectonics and down-faulting along NE-dipping and SW-dipping normal faults that border the massif to the NNE and to the SSW, respectively.

65 The Matese massif is made up of successions of Meso-Cenozoic carbonate rocks with sedimentary facies varying from shallow-water carbonate platform in the south to by-pass margin and slope-to-basin transition facies in the north. The arrangement of the Meso-Cenozoic sedimentary facies was controlled by Jurassic normal faults, striking mostly E-W, that determined the progressive transition from a persistent structural high in central-southern Matese to deep basin conditions in northern Matese. The Cretaceous, Jurassic or Triassic carbonate successions are covered discontinuously by Upper Miocene

70 hemipelagic and turbiditic siliciclastic deposits related to the Apennine orogeny (D'Argenio et al., 1973; Di Bucci et al., 1999; Patacca and Scandone, 2007 with references).

Late Miocene - Pliocene Apennine compression deformed the Meso-Cenozoic units via NE-directed shortening, generating S-dipping reverse faults and NNE-to-N-verging folds and monoclines. The geometry of compressional structures was largely conditioned by the pre-existing E-W faults. The Mio-Pliocene compressional structures are post-dated by Quaternary high-

75 angle normal faults. Normal faulting dissected the western side of the Matese Mt.s since Early Pleistocene, produced a massive deposition of slope-derived breccias, and formed the Venafro and Alife depressions along the Volturno River valley (Ferranti et al., 1996; Brancaccio et al., 1997; Calabrò et al., 2003). The early stages of crustal extension (Early-Middle Pleistocene) were characterized by the formation of major SW-NE-trending structures such as the Garigliano graben, which hosts the Roccamonfina volcano west of the Matese ridge, and the Venafro basin on the north-western side of Matese. There is also

80 evidence of Middle Pleistocene volcaniclastic sediments faulted by SW-NE-striking normal faults originated during this phase of NW-SE-oriented extension (Amato et al.. 2014, 2017; Boncio et al.2016). During this stage, inherited E-W-striking Mesozoic normal faults were reactivated with left-lateral normal-oblique kinematics (Boncio et al., 2016).

After the NW-SE-directed extension, normal faulting driven by SW-NE extension became dominant in the Middle Pleistocene, generating major NW-SE-striking faults and reactivating pre-existing normal and strike-slip faults across the entire Matese

85 area (Ferranti et al., 1996; Calabrò et al., 2003; Di Bucci et al., 2005; Amato et al., 2014). Overall, five major depressions originated due to normal faulting: the Venafro and Ailano depressions to the W and SW, the Isernia and Bojano depressions to the N and NE and the Matese Lake depression in the core of the Matese massif (Fig. 1). The Quaternary extension was accompanied by accumulation of continental deposits within the depressions and along the mountain fronts, including Pleistocene slope-derived breccias, lacustrine and alluvial deposits and large Middle Pleistocene to Holocene alluvial fans

90 (Brancaccio et al., 1997; Di Bucci et al., 2005; Amato et al., 2014; Valente et al., 2019). Middle Pleistocene sediments often contain pyroclastic horizons, mostly deriving from the nearby Roccamonfina stratovolcano (0.55-0.15 Ma activity; Luhr and Giannetti, 1987; Rouchon et al., 2008) and from the Campi Flegrei caldera (39 ka-old Campanian Ignimbrite and 15 ka-old Neapolitan Yellow Tuff; De Vivo et al., 2001; Deino et al., 2004; Giaccio et al., 2017).

2.2 Quaternary tectonics

95 Three main Quaternary normal fault systems can be mapped in the Matese area (Fig. 1): 1) the NE-dipping Northern Matese Fault system; 2) the SW-dipping Aquae Iuliae and Gallo-Letino-Matese Lake Fault systems in central Matese; and 3) the SW-

dipping Southern Matese Fault (SMF) system. The Presenzano - Ailano fault system connects the SMF with the SW-dipping San Pietro Infine fault and allows extensional strain to be transferred to the west.

Late Quaternary faulting and Holocene surface faulting associated with historic or pre-historic earthquakes are known for the

100   Northern Matese Fault system (Galli and Galadini, 2003; Di Bucci et al., 2005; Ferrarini et al., 2017; Galli et al., 2017) and for the Aquae Iuliae Fault (Galli and Naso, 2009; Boncio et al., 2016). For the Gallo-Letino-Matese Lake Fault system, evidence of post-compressional Quaternary faulting has been documented using structural geology and tectonic geomorphology analyses (Bousquet et al., 1993; Calabrò et al., 2003; Aucelli et al., 2013; Valente et al., 2019).

The SMF can be divided into the Ailano – Piedimonte Matese fault to the NW, and the Gioia Sannitica fault to the SE (Boncio

105   et al., 2016). The 18 km-long Ailano – Piedimonte Matese fault is in turn divided into the Raviscanina and Piedimonte Matese fault sections. The Raviscanina section is 11.5 km long, strikes NW-SE and progressively bends to ~W-E in the southern part (~1 km SE of the Sant'Angelo d'Alife village). The Piedimonte Matese fault section is 7 km long and strikes from W-E to WSW-ENE. The eastern part of the Piedimonte Matese fault section, striking ~ W-E, has strong geomorphic evidence of Quaternary activity, while the western part, striking WSW-ENE, is less evident due to cover deposits and larger mountain

110   front sinuosity.

Along the Raviscanina section of the Ailano – Piedimonte Matese fault, a post-350 ka throw rate of 0.27-0.30 mm/yr has been documented by Boncio et al. (2016). The strongest geomorphic evidence of Late Quaternary faulting is in the southern part of the section, close to the bend, where Late Quaternary throw rates of ≥0.15 mm/yr have been estimated. Boncio et al. (2016) suggest that the entire SMF may be presently active and possibly responsible for the 346 CE (Current Era) earthquake. Similar

115   conclusions have been drawn by Valente et al. (2019), who estimate a post-Middle Pleistocene throw rate of > 0.2-0.3 mm/yr on the Raviscanina - Piedimonte Matese mountain front. They also suggest that the E-W-striking Piedimonte Matese fault is the youngest and most active fault, while the NW-SE-striking Gioia Sannitica normal fault (called San Potito Sannitico mountain front) is an older, less active Quaternary fault.

2.3 Seismicity

120   Several strong earthquakes struck the Matese region during the last two millennia (346 CE, 847 CE, 1293 M 5.8, 1349 M 6.8, 1456 M 7.2, 1688 M 7.1, 1805 M 6.7; Guidoboni et al., 2019; Rovida et al., 2020). The NE-dipping Northern Matese Faults were responsible for the 1805 earthquake in the Bojano area (Espostito et al., 1987; Cucci et al., 1996; Galli and Galadini, 2003), and possibly for the first shock of the 1456 earthquake sequence (Galli and Galadini, 2003), even though for the latter event a different interpretation has been proposed (Fracassi and Valensise, 2007).

125   The location of the ancient 847 CE earthquake is highly uncertain. In the CFTI5Med catalogue (Guidoboni et al., 2019), it is located north of the Matese massif, near Isernia. According to Bottari et al. (2020), the macroseismic area could be larger, and the source located significantly SW of the CFTI5Med epicenter, possibly on the Aquae Iuliae fault, as suggested by Galli and Naso (2009), or on the SMF system.

The 1349 earthquake has been associated to the SW-dipping Aquae Iuliae fault on the basis of paleoseismologic investigations
130   (Galli and Naso, 2009), while the sources responsible for the 1293 and 1688 earthquakes in southern Matese are still unknown.
A strong ancient earthquake is known to have seriously damaged the area E, W and SW of the Matese massif in 346 CE, but
the causative fault is unknown. Only hypothetical associations to the Aquae Iuliae fault (Galli and Naso, 2009) or to the SMF
system (Boncio et al., 2016; Valente et al., 2019) have been proposed.

Since 1980, there have not been strong earthquakes associated with a fault in the southern Matese. The largest recorded
135   earthquake occurred in 2013 (Mw 4.9) within the core of the south-eastern Matese massif, at a depth of 10-20 km (Ferranti et
al., 2015). The focal mechanism indicates normal faulting on NW-SE-striking normal faults, nearly parallel to the normal
faults mapped at the surface, but its association to the down-dip prolongation of the outcropping faults is not clear. A small-
magnitude event occurred in 2016 (Mw 4.1), ~10 km NE of the Northern Matese Fault system, at depths shallower than ~10
km. The 2013 and 2016 earthquakes share a common SW-NE-oriented direction of extension, which is consistent with
140   directions obtained from structural geology of Late Quaternary normal faults (Ferranti et al., 2015; Boncio et al., 2016;
Ferrarini et al., 2017) and GPS data (Ferranti et al., 2014; D'Agostino, 2014; Carafa et al., 2020).

3 Materials and methods

3.1 Field geology

Geological mapping was based on a traditional field survey supplemented with a digital survey on a GPS-integrated digital
145   mapping suite (Field Move Software Suite, Petroleum Experts). The topographic maps in digital format were made available
by the Campania Regional authority (1:5,000-scale CTR maps). The fault traces and Quaternary units were mapped on a 1 m-
resolution Digital Elevation Model (DEM) from airborne Light Detection and Ranging (LiDaR) made available by the Italian
Ministry of Environment. The LiDaR DEM was used to extract topographic profiles across fault scarps for measuring throw
values. Throw rates across the measured fault scarps were estimated using the age constraints of faulted
150   sediments/morphologies on scarp or on nearby, correlated sites. Two outcrops of fault zones along the Gioia Sannitica fault
and a small hand-dug trench along the Raviscanina fault section of the Ailano – Piedimonte Matese fault were analysed using
a paleoseismologic approach.

3.2 Sample dating

Three tephra layers interbedded within faulted alluvial fan and colluvial sediments were sampled for tephrostratigraphic
155   analysis and $^{40}Ar/^{39}Ar$ dating. Samples were mostly extracted from deeply argillified slightly indurated to lithified deposits.
They were repeatedly washed in deionized water in order to remove the clay fraction, then treated with at least four,10 minutes-
long ultrasonic washing with renewal of water. The clasts were dried and sieved at 1-phi intervals, finally a lithological
component analysis was carried out on the 1 and 2 phi fractions under a binocular microscope. Unfortunately, no well-
preserved glass fragment survived washing pre-treatment and hence chemical composition of glass could not be achieved. The

160   coarsest and best preserved sanidine phenocrysts were extracted from the three samples for $^{40}Ar/^{39}Ar$ dating. Single crystal

fusions were performed at the University of Wisconsin-Madison. Isotopic analyses were conducted using a Noblesse multi-

collector mass spectrometer (Jicha et al., 2016). The weighted mean ages listed in Tab. 1 are calculated relative to the 1.1864

Ma Alder Creek sanidine standard. Complete $^{40}Ar/^{39}Ar$ analytical data are provided in Tab. S1 of the supplementary material.

The radiocarbon dating was performed on charred material or bulk organic sediments using Accelerator Mass Spectrometry

165   (AMS)   technique   in   the   laboratories   of   Beta   Analytic   (www.radiocarbon.com/)   and   CEDAD   (Italy,

http://www.cedad.unisalento.it/en/) (Tab. 2).

3.3 Paleosol analysis

Macro/micro-morphological and geochemical analyses were conducted on a paleosol that developed on an altered tuff which

was faulted by the Gioia Sannitica fault. Physical and chemical analyses (soil texture, pH (H2O), organic matter content, and

170   cation exchange capacity (CEC)) were performed on air-dried, and sieved (< 2 mm) fraction of the bulk sample of each soil

horizon (van Reeuwijk, 2002; Burt, 2004). Micro-morphological observations were made on thin sections (10 cm x 5 cm x 30

μm) from undisturbed soil samples. Selective extraction techniques were used to determine different forms of Al, Fe and Si

such as acid ammonium oxalate extractable, Alo, Feo and Sio (Schwertmann, 1964), sodium pyrophosphate extractable, Alp

(Bascomb,1968) and dithionite-citrate-bicarbonate extractable iron pool, Fed (Mehra and Jackson,1960). Their amount was

175   measured using atomic absorption spectroscopy (AAS) on the fine earth fraction (< 2 mm). The total iron content, Fet, was

analysed using a Rigaku Supermini X-ray fluorescence (XRF) spectroscopy. These data were used to calculate pedogenetic

indices, shown in Tab. S2 of supplementary material, to estimate the andic properties of the paleosol (ICOMAND, 1988; Parfitt

and Wilson, 1985; Tangari et al., 2018) and the degree of soil maturity (e.g., Arduino et al., 1984; Scarciglia et al., 2018).

4 Geology of the Gioia Sannitica normal fault

180   The Gioia Sannitica normal fault (GF) has been mapped in detail along the piedmont of the southern Matese ridge (Fig. 2). A

detailed geologic map with cross sections is available as supplementary material in Plate S1. Plate S1 contains the synthetic

stratigraphic logs of numerous shallow-depth drill holes used to constrain the Quaternary stratigraphy. The fault can be divided

into two fault sections, on the basis of fault geometry, Quaternary geology and geomorphology of the hanging wall and footwall

blocks: the San Potito section to the north and the Castello di Gioia section to the south.

4.1 Geomorphology and stratigraphy of the southern Matese piedmont along the GF

The GF originates a mountain front along the foot of the south-western slopes of the Matese carbonate ridge, striking on

average N130° in the northern part (San Potito fault section) and N155° in the southern part (Castello di Gioia fault section),

with a ~2 km-wide embayment in between (M. Erbano embayment; Fig. 2). The range slopes moderately (25-40°) down to

the mountain front, without sharp, steep faceted spurs. A mountain front sinuosity of 1.64, typical of slow mountain front

190   activity (Bull, 1987), has been calculated by Valente et al. (2019) in the northern part (San Potito mountain front). The slope profile is straight to concave (see Fig. 2 and geologic sections in Plate S1), suggesting a poorly active or low-uplift-rate range front. However, low linear scarps at the mountain front rise from the gently dipping slopes, indicating recent rejuvenation due to normal faulting.

Different generations of entrenched and overimposed alluvial fans and slope deposits accumulated in the hanging wall of the

195   GF. Alluvial fans cover the bedrock units in the hanging wall of the GF in the northern part (San Potito section), where the top surfaces of alluvial fans slope gently to the SW down to the adjacent Alife plain. Isolated outcrops of carbonate or siliciclastic pre-Quaternary bedrock arise from the piedmont, suggesting that the alluvial fans prograded into a morphologically articulated substratum. The hanging wall of the southern Castello di Gioia section is in general less depressed than the northern counterpart. Continental deposits are less diffuse and confined closer to the fault trace.

200   The morpho-stratigraphic relations among the mapped Quaternary units are shown in Fig. 3. The unit ages are based on volcanic layers and buried paleosols dated in this work, integrated with chronologic determinations in the Ailano – Piedimonte Matese continental succession from previous works (Boncio et al., 2016; Valente et al., 2019) and regional-scale correlations with the Quaternary basins around the Matese massif (Brancaccio et al., 1997; Amato et al., 2014, 2017). We have distinguished two generations of slope-derived deposits (units sd1 and sd2) and four generations of alluvial fan deposits (units

205   U1, U2, U3 and U4), interfingering with coeval fluvial (al) or lacustrine (lac) deposits in the Volturno river plain.

Units sd1 and U1 are made up of carbonate slope-derived breccias and dense to poorly cemented alluvial fan gravels, respectively. Slope breccias crop out only at the base of carbonate slopes, often faulted against the Triassic dolostones. From a sedimentologic point of view, these deposits can be correlated with the Early-Middle Pleistocene slope-derived breccia cropping out widely along the fault-controlled range front in the Volturno River valley, in the Venafro basin, in the Prata

210   Sannita area (Brancaccio et al., 1997; Amato et al., 2017), and in the Letino - Matese Lake area (Aucelli et al., 2013). In particular, the oldest mapped deposits are the well-cemented angular breccia of unit sd1, which can be reasonably correlated with the Lower Pleistocene slope breccias of the Laiano Synthem (Carannante et al., 2011), described by Amato et al. (2018) in the Calore River area, about 20 km SE of the GF.

In the upper part of the U1 alluvial fan gravels, we sampled two layers of distal tephra containing altered leucite-bearing

215   pumice fragments and sanidine crystals which give $^{40}Ar/^{39}Ar$ ages of 564.5 ± 2.1 ka (sample S-227; Tab. 1) and 508.5 ± 0.9 ka (sample S228-F2) (see Tab. S1 of the supplementary material for complete $^{40}Ar/^{39}Ar$ data). Unit U1 is coeval, at least in part, with the Ailano lacustrine deposits (Valente et al., 2019) and can be correlated with the lacustrine-fluvial unit MU1 described in the Venafro basin, about 30 km NW of the GF, by Amato et al. (2017), who dated the upper part of the unit to ~475 ka old. Therefore, based on dated tephra and regional correlations, the succession formed by units sd1 and U1 can be

220   considered to be part of the Early Pleistocene to Middle Pleistocene (older than ~450 ka), with sd1 and U1 that are possibly etheropic each other in the lower part of the succession (Fig. 3).

Unit U2 is made up of heterometric carbonate alluvial fan gravels in a brown silty-sandy matrix with interlayers of decimetre-thick dark brown leucite-free tuffs and thicker pedogenic layers observed in the field and in numerous boreholes (Plate S1). In

the light of their stratigraphic position (younger than U1 unit) and of the fact that Low K-Series leucite-free explosive products
225 of the 35 km-far Roccamonfina volcano are younger than 330 ka (Lower White Trachytic Tuff, Quidelleur et al., 1997), these
leucite-free tuffs can be tentatively correlated with the White Trachytic Tuff (Luhr and Giannetti, 1987). So, the age of this
unit reasonably ranges from Middle to Late Pleistocene.

Units sd2 and U3 are made up of slope-derived colluvial and alluvial fan gravel deposits, respectively. Colluvial deposits sd2
are made up of poorly organized gravels in a brown sandy matrix with dark silty-sandy pedogenic layers. A buried paleosol
230 cropping out ~1.4 km ENE of San Potito Sannitico within the colluvial unit has been dated 43.3 – 42.2 ka old (calibrated age
Before Present, cal. BP; Tab. 2), thus indicating that colluvial gravels accumulated during the glacial periods of Late
Pleistocene. Alluvial fans of Unit U3 slope gently down to the Alife plain and the distal fans interfinger with the alluvial
deposits of the Volturno River, containing the ~40 ka-old Campanian Ignimbrite (Valente et al., 2019). Unit U4 is made up of
Holocene small alluvial fans and coeval brown colluvial deposits and slope debris.

4.2 Geometry, kinematics and fault scarp morphology

235

The GF extends from the Piedimonte Matese town to the south-western slopes of M. Monaco di Gioia, for a total length of
~11.5 km (Fig. 4). The northern San Potito fault section is ~5.5 km long. The southern Castello di Gioia fault section is about
3.5 km long. A ~2 km-long subdued fault scarp connects the San Potito and Castello di Gioia sections across the M. Erbano
embayment. A sharp bend from NW-SE to ~W-E directions connects the GF with the Ailano – Piedimonte Matese fault. To
240 the south, a ~1 km-wide gap separates the GF from a SW-dipping normal fault, with poor geomorphic evidence of recent
activity, that delimits to the west the small M. Acere carbonate ridge.

4.2.1 San Potito fault section

The average strike of the San Potito section is N130°. At a detailed view, the fault trace is formed by longer strands striking
NW-SE, separated by short strands where the fault bends to ~W-E. Striated fault planes at the base of carbonate scarps crop
245 out discontinuously in the northern, central and southern part of the fault trace (Fig.s 5a, b and c). The slip vectors plunge to
SW and SSW, determining normal dip-slip to left-lateral normal-oblique kinematics; close to the southern part of the fault
section (Criscia, S of Fig. 5c) the fault bends to E-W and the kinematics is normal with right-lateral component (WSW-
plunging slip vectors) (see Tab. S2 of the supplementary material for data points of structural data).

The fault displaces Late Miocene siliciclastic deposits, observed in outcrop and drilled by boreholes, against the Cretaceous
250 or Late Triassic-Jurassic carbonate bedrock (Fig. 4 and Plate S1). The geological displacement is likely very large, but the
amount of vertical throw cannot be constrained, as the Miocene siliciclastic rocks unconformably overlie Cretaceous or
Jurassic carbonate rocks, indicating that the pre-Miocene bedrock was already faulted, and the morphology already articulated
at the time of the Miocene siliciclastic sedimentation. Pre-Miocene faulting occurred on faults striking from SW-NE to ~W-
E. It is also likely that NW-SE striking normal faults, including the GF itself, were already formed before the Miocene
255 siliciclastic sedimentation, as testified by the different pre-Miocene bedrock in the hanging wall and footwall blocks of the GF

fault (Cretaceous in the hanging wall, Late Triassic-Jurassic in the footwall). Therefore, the total displacement was accumulated both before and after the Late Miocene. A throw of ~340 m, postdating the base of the Late Miocene siliciclastic deposits, can be estimated in the southern part of the San Potito fault section (Criscia; cross section 2 in Fig. 4). In the same place, Early (?) Pleistocene slope breccia hangs 75-100 m above the fault trace, in the footwall, thus indicating that throw >75-

260   100 m was accumulated in the Quaternary. In the central part of the fault, the total geological throw is estimated to be > 1000 m (cross section C in Plate S1; Fig. 4).

Sharp changes in slope between the carbonate bedrock and the continental cover, and fault scarps on both bedrock and continental deposits have been observed in numerous places along the fault trace. Particularly informative is the site located ENE of San Potito Sannitico (see Fig. 2b), where the fault forms a 5 m-high scarp, measured on the 1-m resolution LiDaR

265   DEM, on Upper Pleistocene slope colluvial deposits of Unit sd2 (Fig. 6). Slope deposits contain a buried paleosol dated to 43.3 – 42.2 ka (cal. BP; Tab. 2), indicating that the upper part of the succession accumulated during the Last Glacial Maximum (LGM), when large volumes of coarse-grained sediments accumulated at the piedmont of the Apennine ridges (e.g., Giraudi and Frezzotti, 1997). The displacement of the topographic surface accumulated after the sedimentation of the LGM deposits, that is after ~15±3 ka ago (Giraudi and Frezzotti, 1997; Roberts and Michetti, 2004). Thus, the average throw rate is 0.35±0.07

270   mm/yr for the last ~15±3 ka.

Figure 7 shows topographic profiles across the GF fault scarp extracted from the 1 m-resolution LiDaR DEM (profiles 1 to 10, location in Fig. 4). Table 3 summarizes the throws measured on topographic profiles across fault scarps, and the deduced throw rates on the base of the estimated age of faulted morphologies/sediments. In particular, east of Piedimonte Matese, at the foot of the M. Olnito slope, late Quaternary colluvial deposits of unit sd2 and a small valley (profile 1 in Fig. 7) are faulted and

275   uplifted in the footwall of a ~3 m-high fault scarp, indicating post-LGM slip rates of ~0.21±0.04 mm/yr. A ~36 m-high fault scarp is measured along profile 3, with gravels of Middle Pleistocene unit U1 in both hanging wall and footwall that suggest post-U1 (i.e., post-450 ka) throw rate of > 0.08 mm/yr. The same fault trace forms a ~4 m-high fault scarp, across a ~15 m-wide zone, on the floor of a Holocene alluvial plain (profile 4) that can be the result of cumulated late Holocene surface faulting events. South of the fault scarps illustrated in Fig. 6, two synthetic splays form a ~14.5 m-high cumulative fault scarp formed

280   after the sedimentation of U1, indicating post-450 ka throw rates >0.03 mm/yr (profile 9). Further to the south, the two splays merge into a single trace forming a small scarp inferred to be post-LGM (2.5 m, profile10).

4.2.2 Castello di Gioia fault section

The Castello di Gioia section strikes on average N155° at the foot of the Mt. Monaco di Gioia slope, with a simple, linear fault trace. Striated fault planes crop out in the central part of the fault trace (Fig. 4: Figs. 5d). The slip vectors plunge to WSW,

285   determining normal kinematics with slight right-lateral component; in one site, both S- and SW-plunging slip vectors have been observed.

The fault displaces Late Miocene siliciclastic deposits against Late Triassic dolostones, with vertical geological separation exceeding 1000 m (Plate S1, section F). It is likely that such a large total geological displacement was accumulated both before

and after the Late Miocene, similar to the San Potito fault section. Near Castello di Gioia, the Early (?) Pleistocene slope
290 breccia of Unit sd1 hangs ~ 80-100 m in the footwall of the fault, indicating that this throw was accumulated in the Quaternary
(Fig. 7, profile 12).

In the M. Erbano embayment, NW-SE-striking Quaternary normal faults displacing the pre-Quaternary bedrock and the Early
(?) Pleistocene sd1 slope breccia has been mapped. The fault crossed by profile 11 (Fig. 7) is characterized by a ~18 m-high
fault scarp with sd1 breccia in both hanging wall and footwall, with no additional evidence of Late Quaternary activity.

295 The connection between the Castello di Gioia and San Potito fault sections is poorly constrained and is inferred here (geologic
map in Plate S1) on the basis of displacement of pre-Quaternary bedrock and escarpments on the Early (?) Pleistocene sd1
slope breccia between the terminations of the Castello di Gioia and San Potito fault traces.

Fault scarps on slopes covered by continental deposits of the units U1 and sd1 have been observed in the central part of the
Castello di Gioia section. The scarps have heights on the order of 4 to 7 m and interrupt the regular, gently-dipping slopes of
300 the M. Monaco di Gioia piedmont (profiles 13, 14 and 15 in Fig. 7). This indicates that the scarp formed after the sedimentation
of unit U1, and likely after the LGM erosion of the mountain slopes, similar to what is observed along the San Potito section.
Thus, the inferred post-LGM throw rates are on the order of 0.28-0.45 mm/yr (Tab. 3).

The Castello di Gioia fault section has been mapped up to the Faicchio area, where geologic and geomorphic evidences of
Late Pleisocene – Holocene faulting dissipate. Here the M. Monaco di Gioia mountain front, in the footwall of the Castello di
305 Gioia fault section, suddenly bends from NW-SE to WNW-ESE and, further to E, to WSW-ENE, for a total length of ~ 8 km
(Fig. 2). The mountain front is controlled by a S-dipping normal fault that appears to be capped by Early-Middle Pleistocene
deposits of the sd1 and U1 units. Further to the SE, a SW-dipping normal fault can be inferred along the SW slope of the M.
Acero Jurassic-Cretaceous carbonate ridge (Fig. 2; Plate S1). A ~1.2 km-wide step-over separates the M. Acero fault from the
Castello di Gioia fault section. We could not observe fault planes or scarps or other evidence of Late Pleistocene – Holocene
310 activity along the M. Acero fault trace.

5 Late Pleistocene – Holocene surface faulting

5.1 The San Potito site on the Gioia Sannitica Fault

In the central-southern part of the San Potito fault section, the fault is formed by two parallel splays (Fig. 4). The eastern splay
separates the continental deposits from the dolomitic bedrock, while the western splay is within the continental deposits. Across
315 the western splay, a ~40 m-long cut along a dirty road was accurately cleaned and logged for analysing two fault zones, one
located in the footwall of the splay (Fault zone 1, Fig. 8) and one located on the main trace of the splay (Fault zone 2, Fig. 9).
Fault zone 1 (Fig. 8) is formed by two SW-dipping normal fault strands, F1 and F2. F2 separates poorly-organized, coarse,
white gravels in the footwall (unit 1, corresponding to unit U1 of the geologic map in Fig. 4 and Plate S1), from a succession
of stacked, matrix-rich colluvial gravel units in the hanging wall (units 4 to 7).

320 Unit 1 contains a 20 cm to 40 cm-thick layer of yellow (lower part) to yellowish grey (upper part) distal tephra (unit 2) containing yellowish glass aggregates, poorly preserved leucite-bearing grey pumice fragments, loose crystals of rare sanidine that are dated to 564.5 ± 2.1 ka (sample S-227; Tab. 1; Tab. S1), brown and minor green clinopyroxene and few dark mica grains, and a lithic fraction formed by leucite-bearing lava fragments.

Colluvial units 4, 5 and 6 are faulted in the hanging wall of fault F2. The youngest faulted unit is unit 6, the fine-grained matrix

325 of which has been dated 1,377-1,126 yrs BCE (Before Current Era, calendar calibrated age; sample S227_5-1, Tab. 2).

Fault zone 2 (Fig. 9) is formed by three main SW-dipping normal fault strands (F3, F4 and F5). Fault F3 separates organized, coarse, white gravels in the footwall (unit 1, corresponding to unit U1 of the geologic map in Fig. 4 and Plate S1), from a succession of colluvial gravels (unit 2) covered by a thick body of brown distal tephra (unit 3). The tephra contains whitish to grey glass aggregates and rare, very altered pumice fragments with leucite crystals, loose crystals of abundant sanidine and

330 minor green and brown clinopyroxene grains, and a lithic fraction with limestone and rare leucite-bearing lava fragments. The sanidine crystals have been dated to 508.5 ± 0.9 ka (Tab. 1; Tab. S1).

The tephra unit is trapped within the main fault zone, between F3 and F5, and the original geometry cannot be reconstructed due to synthetic and antithetic faulting and erosion. The top of the tephra unit, in the hanging wall of fault F4, is altered by a paleosol buried by coarse, non-organized, white gravels (unit 4), likely deriving from erosion and colluviation of unit 1. The

335 buried paleosol has the appearance of volcanic soils with andic properties. In detailed analysis (see Text S1 and Tab. S4 for a detailed description), the paleosol shows weak andic properties and poor pedogenetic evolution, suggesting a young age (Late Pleistocene – Holocene), and possible disturbance by erosional ad colluvial processes. These findings are consistent with radiocarbon dating of the bulk organic fraction of the paleosol, which gave ages of 6,510 – 6,250 yrs BCE (Tab. 2).

The paleosol and the overlying unit 4 are faulted by F4 and F5. In the hanging wall of F5, a sequence of colluvial units crops

340 out. The lack of organic material prevented any attempt of dating unit 4. Unit 5 differs from unit 4 due to average larger percentage of boulders, and for the presence of brown, sandy matrix. Radiocarbon dating of the bulk organic fraction within the matrix of Unit 5 gave unrealistic young ages (post-1,950 CE; Tab. 2, sample 228_7-1), suggesting contamination with young carbon.

Two wedge-shaped colluvial units (units 6 and 7) are present between units 4-5 and the modern soil. Unit 6, formed by material

345 from unit 4, seals a fault zone of F5, and is faulted by the western, shallowest strand of F5. The geometry and facies of unit 6 suggest that this unit sedimented after a period of erosion of units 4, 5 and 4b (fault zone), and accumulated close to F5, possibly during a cold period for the lack of organic sediment. The wedge-shaped geometry of unit 6, thickening towards F5, suggests that the sedimentation was sourced by a fault scarp that exposed unit 4 in the footwall of F5, possibly after a surface faulting event (scarp-derived colluvial wedge). The colluvial wedge was then faulted by the western splay of F5. Unit 7 is a

350 wedge-shaped, gravel unit rich in dark brown organic matrix with charcoals dated 1,445 – 1,625 yrs CE (Tab. 2, sample 228_1ter). The wedge thickens sharply in the hanging wall of F1 and seals a steep scarp formed by F5, with unit 4 in the footwall. There is no evidence of faulting of unit 7. The geometric arrangement suggests that unit 7 deposited shortly after the

most recent surface faulting event on F5. There is no evidence for pedogenic processes between units 7 and unit 6, suggesting that the wedge-shaped colluvial unit 7 deposited after a period of erosion or with negligible pedogenesis.

355   A ~1 m-high eroded scarp across the F3-F5 fault zone is visible on a detailed topographic profile of the ground surface, supporting the interpretation of surface faulting. Though the complex architecture of the fault zone prevents any reliable restoration, the buried paleosol between units 3 and 4 provides insights on the minimum Holocene vertical displacement. The paleosol is vertically displaced of >1.1 m by F4 and >1.3 m by F5 (total throw >2.4 m), indicating average throw rate >0.29 mm/yr for a period of 8,145 yrs (largest age range between age of faulted paleosol and age of unfaulted unit 7).

360   **5.2 The Sant'Angelo d'Alife trench site on the Ailano – Piedimonte Matese Fault**

A small trench was dug across the southern part of the Raviscanina fault section (see Fig. 2 for location) in order to build upon previous work (Boncio et al., 2016) and obtain additional age constraints on the APMF activity.

The trench crosses a fault zone formed by a main fault (F1) and a synthetic splay (F2) (Fig. 10). Fault F1 separates cataclastic dolostone in the footwall (unit 1) from high-strength, light grey-to-light brown tuff pervasively cut by fault-parallel veins of

365   calcium-carbonate concretions (unit 2). Unit 2 is truncated upwards by an erosional surface and covered by reddish-brown, clayey colluvium containing sparse carbonate clasts (unit 4) faulted by F1 and F2. Radiocarbon dating of two samples from unit 4 gave Holocene ages, but with significantly different dates, varying from 770 - 660 yrs CE (sample C1_D-E) to 908 – 805 yrs BCE (sample C8_D-W), indicating large age uncertainty, possibly due to contamination by young carbon in sample C1_D-E. Unit 4 is covered by a wedge-shaped colluvial unit formed by light brown silty-sand matrix with abundant cataclasite

370   clasts deriving from the F1 fault rock (unit 5). The matrix of unit 5 has been dated 1,270 – 1,385 yrs CE (samples C3_D-E and C7_D-W; Tab. 2). Unit 5 is not faulted. Possibly, this unit formed after the fault rock was exposed to weathering and erosion due to a surface faulting event (scarp-derived colluvial wedge).

Fault F2 displaces vertically the bottom of unit 4 by ~30 cm. In the hanging wall of F2, unit 4 covers a 188.8 ± 3.0 ka old colluviated tephra unit (unit 3) made up of very altered whitish to yellowish pumice fragments, abundant loose sanidine crystals

375   and rare green and brown clinopyroxene crystals, together with several opaque grains in the finer fraction (sample C9-DO; Tab. 1; Tab. S1). Unit 3 is colluviated, therefore it is younger than the obtained ages.

The total, minimum vertical displacement accumulated by unit 4 is estimated to be ~0.8 m, corresponding to the maximum vertical thickness of unit 5 (~0.5 m; the space created by surface faulting and filled by the colluvial wedge) plus the 0.3 m of displacement on F2. This suggests average throw rate >0.35 mm/yr for a period of 2,285 yrs (largest age range between age

380   of faulted unit 4 and age of unfaulted unit 5).

6 Seismotectonic implications: segmentation, throw rates and earthquake potential

6.1 Overall architecture and kinematics

In Fig. 11, the GF is mapped together with all the other known Matese normal faults (from Di Bucci et al., 2005; Galli and Naso, 2009; Boncio et al., 2016; Ferrarini et al., 2017; Galli et al., 2017). The available age constraints are summarized in Fig.
385 11b. A summary of fault geometry (strike, dip) and kinematics (slip vector trend) is presented in Fig. 12. Overall, the present architecture of the SMF system is characterized by major NW-SE-striking faults (Raviscanina section of APMF and GF) with a nearly E-W fault in between (Piedimonte Matese section). The prevailing measured strikes range between 115° and 140°. Variations to E-W strike (95-105°) are measured at smaller scale within major NW-SE faults (Fig. 12a). Note that in Fig. 12a the ~E-W Piedimonte Matese section is under-sampled due to poor exposure of the fault. Dip angles are mostly within the
390 range typical of high-angle normal faults (60-80°, Fig. 12b). Fault kinematics is uneven along strike. The trend of slip vectors varies from 270° to 110°, with prevailing slip vectors plunging to SW (200-240°) and to SE (110-180°). SW-plunging slip vectors are consistent with the direction of active regional extension obtained from focal mechanisms and GPS velocity vectors (210-240°, Fig. 12c; Fig. 1). Interestingly, both SW-plunging and SE-plunging slip vectors are recorded on NW-SE, E-W and WSW-ENE faults. This pattern cannot be explained by simple models of normal fault growth, even considering variations due
395 to slip vector convergence towards the fault center during fault growth (Roberts, 1996; Roberts and Michetti, 2004). It seems more likely that this pattern is the result of repeated reactivations of pre-existing faults, as proposed by Boncio et al. (2016) and Amato et al. (2017). SE-plunging slip vectors were recorded mostly during the NW-SE extensional phase that opened the Garigliano graben in the Early-Middle Pleistocene, when new NE-striking normal faults formed, and pre-existing Jurassic E-W normal faults, and pre-Miocene or pre-Quaternary NW-SE normal faults have been reactivated with left-lateral normal-
400 oblique kinematics. The mutual relationships among fault segments with different orientation and the overall geometry of the system probably evolved through time, depending on the dominant extensional direction. The present overall architecture shown in Fig. 11b was likely achieved during the latest stage of extension, dominated by NE-directed stretching, operating since Middle Pleistocene and still active.

6.2 Throw rates

405 The GF is characterized by low Late Pleistocene – Holocene throw rates, ranging from 0.21 mm/yr to 0.49 mm/yr (Tab. 3; Fig. 11b).
The bedrock and Quaternary geology of the area indicates that the GF, and in general all the normal faults of the SMF system, have a long tectonic history that started before the syn-orogenic sedimentation of Late Miocene flysch, and continued after the Mio-Pliocene compressional tectonic phase and persisted for the entire Quaternary. The mature geomorphology of the southern
410 Matese mountain front, indicated by straight-to-concave mountain slopes, poorly faceted front, entrenched alluvial fans (this work and Valente et al., 2019), might be the result of the combined long pre-Quaternary and Quaternary geomorphological evolution and average low-rate tectonic rejuvenation. The throw rate is in any case sufficient to determine clear morphotectonic

markers of young fault activity, mostly in the form of metric-scale post-LGM scarps. Another possible explanation can be a recent resurrection, or acceleration, of fault activity after a period of inactivity or of very low slip rate.

6.3 Seismogenic potential

The detailed field survey presented here along the GF revealed Late Pleistocene and Holocene faulting. The identification of colluvial wedges sedimented in close relation with fault activity (e.g., Fig 9) and the occurrence of post-LGM meters-scale scarps and smaller scarps on Holocene alluvium (Fig. 7) indicate that the GF is capable of producing surface faulting events during moderate-to-strong earthquakes.

Given the geologic evidence of fault activity, two questions arise for the GF and APMF: how large is the expected earthquake potential? Is there any historical earthquake that can be associated to these faults?

Concerning the earthquake potential, fault lengths and the derived estimated magnitudes obtained from various empirical relationships available in the literature (Wells and Coppersmith, 1994; Pavlides and Caputo, 2004; Wesnousky, 2008; Galli et al., 2008) are summarized in Tab. 4. The obtained values assume that the entire mapped fault length will rupture during the earthquake. The lengths of GF and APMF taken separately are 11.5 km and 18 km, respectively. Due to the poor geologic and geomorphic evidence of recent activity for the Piedimonte Matese section of the APMF, we have considered separately also the Raviscanina fault section (length 11.5 km). The average estimated magnitudes are M 6.2, M 6.2 and M 6.5 for the GF, Raviscanina fault section and entire APMF, respectively. Assuming a rupture of both the APMF and GF (length of 19.5 km), the estimated average magnitude is M 6.8.

The data collected in the San Potito and Sant'Angelo d'Alife sites give insights on possible association of historical earthquakes to the faults (Fig. 11a and 11c); some possible rupture scenarios compatible with dates of historical earthquakes are proposed in Tab. 4. The association of the 1688 large earthquake (M 7.1) can be excluded, as the last surface faulting event on both GF and APMF occurred before 1688. The youngest wedge-shaped colluvial units in the two studied sites can be interpreted as scarp-derived colluvial wedges (CW in Fig. 11c), sedimented in the hanging wall of the free face shortly after surface faulting events (e.g., McCalpin, 2009). The ages of the CWs are similar in both sites, suggesting that APMF and GF could have been activated during the same event, or during two events close in time. The event(s) is(are) compatible with the 1349 or 1293 earthquakes, or both. The strong 1349 event (M 6.8) has been associated to the Aquae Iuliae fault, located 4.5 km N of the APMF (Galli and Naso, 2009). An activation of the APMF and/or GF during the 1349 event cannot be excluded. The Aquae Iuliae fault is not a long fault (~20 km in Galli and Naso, 2009; 16.5 km in Boncio et al., 2016), and a longer rupture can better match the estimated magnitude (rupture ~>30 km for M = 6.8). Nevertheless, the damage is distributed mostly to the NW of the Aquae Iuliae fault, and not to the SE as expected in case of an activation of the APMF and/or the GF (Fig. 11a). Therefore, an association of the 1349 earthquake to the APMF and/or GF is not preferred. An activation of the GF and/or APMF during the 1293 earthquake seems plausible. The earthquake is constrained by a few data points, with heavy damage documented 20 km north (Intensity IX) and 18 km south (Int. VIII-IX) of the estimated epicenter (southern Matese; Guidoboni et al., 2019). The estimated magnitude from historical data is moderate (M 5.8), and an activation of the GF alone, located between the two

damaged sites, or the APMF alone, seems plausible. If we assume a reactivation of both the GF and APMF, we should conclude that the historical magnitude probably underestimates the true magnitude of the event.

A second, faulted wedge-shaped colluvial unit is present in the San Potito site, beneath the most recent CW (unit 6 in Fig. 9). Unit 6 fills in an erosional cut and is free of organic matrix, suggesting deposition during a cold, high-energy moment.

450   Assuming that the sediments of unit 6 originated from a fault scarp formed before 1293, the only known earthquake sufficiently large to likely produce surface faulting is the 346 earthquake (Galadini and Galli; 2004; Guidoboni et al., 2019). The cold period during which unit 6 was formed could correspond with the cold period of the High Middle Ages (Giraudi et al., 2011; see grey areas in Fig. 11c). The colluvial unit sourced by the 346 scarp would have been faulted by the 1293 event, with a corresponding inter-event time of ~950 yrs. The thickness of the two colluvial units, measured close to the fault, is ~30 cm,

455   suggesting coseismic surface throw between 30 and 60 cm.

If the macroseismic area of the 847 earthquake is larger than that reported in the CFTI5Med catalogue, and if the epicenter is located WSW of the Matese massif, as proposed by Bottari et al. (2020), this earthquake could be considered the possible source of surface faulting in the studied area. Surface faulting during 847 CE is compatible with the ages of both the San Potito and Sant'Angelo d'Alife sites. Therefore, additional hypotheses on the slip history of the APMF and GF can be formulated.

460   Additional paleoseismological studies could help reduce the uncertainties.

The seismogenic potential estimated in this work, and the likely association to poorly known, ancient historical earthquakes have obvious implications for seismic hazard of this region. In fact, seismic hazard assessments for practical applications (e.g., building design, civil protection; MPS04, Stucchi et al., 2011) are currently based on historical earthquakes of the last millennium, with no possibility of including the effects of older events or of faults able to source long-recurrence earthquakes.

465   Therefore, the seismic hazard of the southern Matese area, and west of it, is probably underestimated.

7 Conclusions

The 11.5 km-long Gioia Sannitica normal fault (GF), at the foot of the southern Matese mountain front, is an active fault showing evidence of surface faulting during the Late Pleistocene - Holocene (post-LGM fault scarps, faulted colluval deposits and paleosols). The GF and the 18 km-long Ailano-Piedimonte Matese fault (APMF) form the 29.5 km-long Southern Matese

470   Fault system. The average slip rate varies along-strike, as expected for normal faults, with largest Late Pleistocene – Holocene throw rates not exceeding ~0.5 mm/yr, indicating a slowly-slipping fault.

The mature mountain front morphology can be explained by low uplift rates, combined with long geologic history of the fault. The onset of fault activity can be dated back to the early Quaternary, and possibly earlier. Multiple slip episodes have been constrained between ~8,500 yrs ago and 1,635 CE on the GF, and between ~2,900 yrs ago and 1,390 CE on the APMF. The

475   two sites are compatible with surface faulting events that could have ruptured the entire Southern Matese Fault system. Activation of the GF and APMF separately is also compatible with the observed displacements. The estimated seismogenic potential for each individual fault are M 6.1 for GF or Raviscanina fault section alone and M 6.5 for the APMF. In case

of rupturing of the entire Southern Matese Fault system, the seismogenic potential would be up to M 6.8. The observed displacements on the GF and APMF are compatible with activations during some poorly known historical earthquakes, such

480 as the 1293 (M 5.8), 1349 (M 6.8; southern prolongation of the rupture on the Aquae Iuliae fault?) and 346 CE earthquakes. A fault rupture during the 847 CE poorly-constrained earthquake is also compatible with the dated displacements.

Data availability

All datasets presented in this study are included in the article and in the supplementary material.

Author contributions

485 PB contributed to conceptualization, funding acquisition, investigation (field mapping), data curation, data analysis, supervision and validation. EA contributed to conceptualization, investigation (field mapping), data curation and data analysis. VA and PA contributed to investigation (field mapping), data curation and data analysis (mostly Quaternary geology and geomorphology). PP analysed the tephra layers. ACT analysed the San Potito paleosol. BRJ performed ^{40}Ar/^{39}Ar experiments for sample dating. PB and EA wrote the original draft, all the authors contributed to review & editing of the manuscript.

Competing interests

490

The authors declare that they have no conflict of interest.

Acknowledgements

This work was funded by Department DiSPUTer, "G. d'Annunzio" University of Chieti, "ex 60%" research funds to P. Boncio. Part of this wok was realized during the PhD project of E. Auciello.

495 **References**

Amato, V., Aucelli, P.P.C., Cesarano, M., Jicha, B., Lebreton, V., Orain, R., Pappone, G., Petrosino, P., and Russo Ermolli, E.: Quaternary evolution of the largest intermontane basin of the Molise Apennine (centralsouthern Italy), Rendiconti Lincei 25, 197–216, https://doi.org/10.1007/s12210-014-0324-y, 2014.

Amato, V., Aucelli, P.P.C., Bellucci Sessa, E., Cesarano, M., Incontri, P., Pappone, G., Valente, E., and Vilardo G.:
500 Multidisciplinary approach for fault detection: integration of PS-InSAR, geomorphological, stratigraphic and structural data in the Venafro intermontane basin (Central-Southern Apennines, Italy), Geomorphology 283, 80–101, https://doi.org/10.1016/j.geomorph.2017.01.027, 2017.

Amato, V., Aucelli, P.P.C., Cesarano, M., Filocamo, F., Leone, N., Petrosino, P., Rosskopf, C.M., Valente, E., Casciello, E.,
Giralt, S., and Jicha, B.R: Geomorphic response to late Quaternary tectonics in the axial portion of the Southern Apennines
505   (Italy): A case study from the Calore River valley,Earth Surf. Process. Landforms, 43, 2463–2480,
https://doi.org/10.1002/esp.4390, 2018.

Arduino, E., Barberis, E., Carraro, F., and Forno, M.G.: Estimating relative ages from iron-oxide/total-iron ratios of soils in
the western Po Valley (Italy), Geoderma 33, 39-52, 1984.

Aucelli, P. P. C., Cesarano, M., Di Paola, G., Filocamo, F., and Rosskopf, C. M.: Geomorphological map of the central sector
510   of the Matese Mountains (Southern Italy): an example of complex landscape evolution in a Mediterranean mountain
environment, Journal of Maps, 9, 604-616, https//doi.org/ 10.1080/17445647.2013.840054, 2013.

Bascomb, C.L.: Distribution of pyrophosphate-extractable iron and organic carbon in soils of various groups, J. Soil Sci., 19,
251–268, 1968.

Boncio, P., Dichiarante, A.M., Auciello, E., Saroli,M., and Stoppa, F.: Normal faulting along the western side of the Matese
515   Mountains: implications for active tectonics in the Central Apennines (Italy), J. Struct. Geol., 82, 16–36,
http://doi.org/10.1016/j.jsg.2015.10.005, 2016.

Bottari, C., Ferranti, L., Di Maio, R., Frisetti, A., De Paola, C., La Manna, M., Piegari, E., and Marazzi, F.: The 847 CE
earthquake in central-southern Italy: New hints from archaeosismological and geophysical investigations in the Volturno River
Valley area, Tectonophysics, 774, 228301, https://doi.org/10.1016/j.tecto.2019.228301, 2020.

520   Bousquet, J.C., Grellet, B., and Sauret, B.: Neotectonic setting of the Benevento area: comparison with the epicentral zone of
the Irpinia earthquake, Ann. Geofis., 36, 245-251, 1993.

Brancaccio, L., Cinque, A., Di Crescenzo, G., Santangelo, N., and Scarciglia, F.: Alcune osservazioni sulla tettonica
quaternaria nell'Alta Valle del F. Volturno. Il Quaternario,10, 321-328, 1997.

Bull, W. B.: Relative rates of long-term uplift of mountain fronts, in: Directions in Paleoseismology, edited by: Crone, A. J.,
525   and Omdahl, E. M., Geol. Surv. of U.S., Open File Rep. 87–673, 192–202, 1987.

Burt, R.: Soil survey laboratory methods manual, in: Soil Survey Investigations Report No 42, Version 4.0, edited by: Burt,
R., United States Department of Agriculture –National Resources Conservation Service (USDA – NRSC), Lincoln, NE. 2004.

Calabrò, R.A., Corrado, S., Di Bucci, D., Robustini, P., and Tornaghi, M.: Thin-skinned vs. thick-skinned tectonics in the
Matese Massif, Central-Southern Apennines (Italy), Tectonophysics, 377, 269- 297, 2003.

530   Carafa, M. M. C., Galvani, A., Di Naccio, D., Kastelic, V., Di Lorenzo, C., Miccolis, S., Sepe, V., Pietrantonio, G., Gizzi, C.,
Massucci, A., Valensise, G., and Bird, P.:Partitioning the ongoing extension of the central Apennines (Italy): Fault slip rates
and bulk deformation rates from geodetic and stress data, Journal of Geophysical Research- Solid Earth, 125, e2019JB018956,
https://doi.org/10.1029/2019JB018956, 2020.

Carannante, G., Cesarano, M., Pappone, G., and Putigniano, M.L.: Note Illustrative della Carta Geologica d'Italia alla scala
535   1:50 000 foglio 431 (Caserta Est),Servizio Geologico d'Italia, ,ISPRA, Roma. 2011.

Chiaraluce, L., Di Stefano, R., Tinti, E., Scognamiglio, L., Michele, M., Casarotti, E., Cattaneo, M., De Gori, P., Chiarabba, C., Monachesi, G., Lombardi. A., Valoroso, L., Latorre, D., and Marzorati, S.:The 2016 central Italy seismic sequence: A first look at the mainshocks, aftershocks, and source models, Seismological Research Letters, 88, 757–771, https://doi.org/10.1785/0220160221, 2017.

540   Cinti, F. R., De Martini, P. M., Pantosti, D., Baize, S., Smedile, A., Villani, F., Civico, R., Pucci, S., Lombardi, A. M., Sapia, V., Pizzimenti, L., Caciagli, M., and Brunori, C. A.: 22-kyr-Long Record of Surface Faulting Along the Source of the 30 October 2016 Earthquake (Central Apennines, Italy), From Integrated Paleoseismic Data Sets, Journal of Geophysical Research-Solid Earth, 124 (8), 9021-9048, https//doi.org/ 10.1029/2019JB017757, 2019.

Civico, R., Pucci, S., Villani, F., Pizzimenti, L., De Martini, P. M., Nappi, R., and the Open EMERGEO Working
545   Group:Surface ruptures following the 30 October 2016 Mw 6.5 Norcia earthquake, central Italy, Journal of Maps, 14, 151–160, https://doi.org/10.1080/17445647.2018.1441756, 2018.

Corniello, A., and Russo, D.: La piana del medio corso del F. Volturno (Campania) Idrogeologia e vulnerabilità all'inquinamento delle falde, in : Atti 1° Convegno Nazionale Protezione e gestione delle acque sotterranee: metodologie, tecnologie e obiettivi, Marano sul Panaro, Modena, 20-22 Settembre 1990, 1, 131-148, 1990.

550   Cucci, L., D'Addezio, G., Valensise, G., and Burrato, F.: Investigating seismogenic faults in Central and Southern Apennines (Italy): modelling of fault-related landscape features, Ann. Geofis., 39, 603-618, 1996.

D'Agostino, N.: Complete seismic release of tectonic strain and earthquake recurrence in the Apennines (Italy), Geophysical Research Letters, 41, 1155–1162. https://doi.org/10.1002/2014GL059230, 2014.

D'Argenio, B., Pescatore, T., and Scandone, P.: Schema geologico dell'Appennino meridionale (Campania Lucania), in:
555   Moderne vedute sulla geologica dell'Appennino, Acc. Naz. Lincei,183,49-72, 1973.

De Vivo, B., Rolandi, G., Gans, P. B., Calvert, A., Bohrson, W. A., Spera, F. J., and Belkin, H. E.: New constraints on the pyroclastic eruptive history of the Campanian volcanic plain (Italy), Mineralogy and Petrology, 73, 47–65, 2001.

Deino, A.L., Orsi, G., De Vita, S., and Piochi, M.: The age of the Neapolitan Yellow Tuff caldera-forming eruption (Campi Flegrei caldera, Italy) assessed by 40Ar/39Ar dating method, Journal of Volcanology and Geothermal Research, 133, 157–
560   170, 2004.

Di Bucci, D., Corrado, S., Naso, G., Parotto, M., and Praturlon, A.: Evoluzione tettonica neogenico-quaternaria dell'area molisana, Boll. della Soc. Geol. Ital., 118, 13-30, 1999.

Di Bucci, D., Naso, G., Corrado, S., and Villa, I.M.: Growth, interaction and seismogenic potential of coupled active normal faults (Isernia Basin, central-southern Italy), Terra Nova, 17, 44-55, 2005.

565   DISS Working Group:Database of Individual Seismogenic Sources (DISS), Version 3.2.1: A compilation of potential sources for earthquakes larger than M 5.5 in Italy and surrounding areas, Istituto Nazionale di Geofisica e Vulcanologia, http://doi.org/10.6092/ INGV.IT-DISS3.2.1.diss.rm.ingv.it/diss/,; , 2018.

Esposito, E., Luongo, G., Marturano, A. andPorfido, S.: Il terremoto di S. Anna del 26 luglio 1805. Mem. Soc. Geol. It., 37, 171-191, 1987.

570   Faure Walker, J., Boncio, P., Pace, B., Roberts, G., Benedetti, L., Scotti, O., Visini, F., and Peruzza, L.: Fault2SHA Central Apennines database and structuring active fault data for seismic hazard assessment, Scientific Data, 8(1), https//doi.org/ 10.1038/s41597-021-00868-0, 2021.

Ferranti, L., Oldow, J.S., and Sacchi, M.: Pre-Quaternary orogen-parallel extension in the Southern Apennine belt, Italy,Tectonophysics, 260, 325-347, 1996.

575   Ferranti, L., Palano, M., Cannavò, F., Mazzella, M.E., Oldow, J.S., Gueguen, E., Mattia, M., and Monaco, C.: Rates of geodetic deformation across active faults in southern Italy. Tectonophysic, 621, 101–122, https://doi.org/10.1016/j.tecto.2014.02.007, 2014.

Ferranti, L., Milano, G., Burrato, P., Palano, M., and Cannavò, F.: The seismogenic structure of the 2013–2014 Matese seismic sequence, southern Italy: implication for the geometry of the Apennines active extensional belt, Geophys. J. Int., 201, 823–

580   837, https://doi.org/10.1093/gji/ggv053, 2015.

Ferrarini, F., Boncio, P., de Nardis, R., Pappone, G., Cesarano, M., Aucelli, P. P. C., and Lavecchia, G.: Segmentation pattern and structural complexities in seismogenic extensional settings: The North Matese Fault System (Central Italy), Journal of Structural Geology, 95, 93–112, https://doi.org/10.1016/j.jsg.2016.11.006, 2017.

Fracassi, U. and Valensise, G.: Unveiling the sources of the catastrophic 1456 multiple earthquake: Hints to an unexplored

585   tectonic mechanism in Southern Italy, Bull. Seismol. Soc. Am., 97, 3, 725-748, https//doi.org/ 10.1785/0120050250, 2007.

Galadini, F. and Galli, P.: The 346 A.D. earthquake (central-southern Italy): an archaeoseismological approach, Annals of Geophysics, 47, 885-905, 2004.

Galli, P. and Galadini, F.: Disruptive earthquakes revealed by faulted archaeological relics in Samnium (Molise, southern Italy), Geophys. Res. Lett.,30 , 1266, https//doi.org/10.1029/2002GL016456, 2003.

590   Galli, P. andNaso, J.: Unmasking the 1349 earthquake source (southern Italy): paleoseismological and archaeoseismological indications from the Aquae Iuliae fault, Journal of Structural Geology, 31, 128-149, https//doi.org/10.1016/j.jsg.2008.09.007, 2009.

Galli, P., Galadini, F., and Pantosti, D.: Twenty years of paleoseismology in Italy, Earth Sci. Rev., 88, 89–117, https://doi.org/10.1016/j. earscirev.2008.01.001. 2008.

595   Galli, P., Giaccio, B., Messina, P., Peronace, E., Amato, V., Naso, G., Nomade, S., Pereira, A., Piscitelli, S., Bellanova, J., Billi, A., Blamart, D., Galderisi, A., Giocoli, A., Stabile, T., and Thil, F.: Middle to Late Pleistocene activity of the northern Matese fault system (southern Apennines, Italy), Tectonophysics, 699, 61–81, http://doi.org/10.1016/j.tecto.2017.01.007, 2017.

Galli, P., Galderisi, A., Peronace, E., Giaccio, B., Hajdas, I., Messina, P., Pileggi, D., and Polpetta, F.: The awakening of the

600   dormant Mount Vettore fault (2016 central 838 Italy earthquake, Mw 6.6): Paleoseismic clues on its millennial silences, Tectonics, 38 , 687-705, doi.org/10.1029/2018TC005326, 2019.

Giaccio, B., Niespolo, E.M., Pereira, A., Nomade, S., Renne, P.R., Albert, P.G., Arienzo, I., Regattieri, E., Wagner, B., Zanchetta, G., Gaeta, M., Galli, P., Mannella, G., Peronace, E., Sottili, G., Florindo, F., Leicher, N., Marra, F. and Tomlinson,

E.L.: First integrated tephrochronological record for the last ~190 kyr from the Fucino Quaternary lacustrine succession, central
605 Italy, Quat. Sci. Rev., 158, 211-234, http://dx.doi.org/10.1016/j.quascirev.2017.01.004, 2017.

Giraudi, C. and Frezzotti, M.: Late Pleistocene glacial events in the central Apennines, Italy, Quaternary Research, 48, 280–290, https://doi.org/10.1006/qres.1997.1928, 1997.

Giraudi, C, Magny, M, Zanchetta, G., and Drysdale, R.N.: The Holocene climate evolution of the Mediterranean Italy: A review of the geological continental data, The Holocene, 21, 105–115, 2011.

610 Guidoboni, E., Ferrari, G., Tarabusi, G., Sgattoni, G., Comastri, A., Mariotti, D., Ciuccarelli, C., Bianchi, M.G., and Valensise, G.: CFTI5Med, the new release of the catalogue of strong earthquakes in Italy and in the Mediterranean area, Scientific Data, 6, 80,, https://doi.org/10.1038/s41597-019-0091-9, (2019).

ICOMAND :Circular Letter No. 10. International Committee on the Classification of Andisols, New Zealand Soil Bureau, Lower Hutt, New Zealand, 1988.

615 Jicha, B.R., Singer, B.S., and Sobol, P.: Re-evaluation of the ages of 40Ar/39Ar sanidine standards and supereruptions in the western US using a Noblesse multi-collector mass spectrometer, Chemical Geology, 431, 54–66, https://doi.org/10.1016/j.chemgeo.2016.03.024, 2016.

Locati, M., Camassi, R., Rovida, A., Ercolani, E., Bernardini, F., Castelli, V., Caracciolo, C.H., Tertulliani, A., Rossi, A., Azzaro, R., D'Amico, S., and Antonucci, A.: Database Macrosismico Italiano (DBMI15), versione 3.0, Istituto Nazionale di
620 Geofisica e Vulcanologia (INGV), https://doi.org/10.13127/DBMI/DBMI15.3,2021.

Luhr, J.F. and Giannetti, B.: The Brown Leucitic Tuff of Roccamonfina Volcano (Roman Region, Italy), Cont. Mineral. Petrol., 95, 420-436, 1987.

McCalpin J. P. (Ed.): Paleoseismology,2nd Edition, International Geophysics 95, Academic Press, 629 pp., 2009.

Mehra, O.P. andJackson, M.L.: Iron oxide removal from soils and clays by a dithionite-citrate system buffered with sodium
625 bicarbonate, Clay Clay Miner., 7, 317-327, 1960.

Min, K., Mundil, R., Renne, P.R., and Ludwig, K.R.: A test for systematic errors in 40Ar/39Ar geochronology through comparison with U/Pb analysis of a 1.1-Ga rhyolite, Geochim. Cosmochim. Acta, 64, 73–98, 2000.

Parfitt, R.L. and Wilson, A.D.: Estimation of allophane and halloysite in three sequences of volcanic soils, New Zealand, in: Volcanic Soils, edited by: Fernandez Caldas, E., and Yaalon, D.H., Catena Supplement 7, Catena Verlag, Braunschweig,
630 Desdedt, Germany, 1–8, 1985.

Patacca, E. and Scandone, P.: Geology of the southern Apennines, Boll. della Soc. Geol. Ital. Spec. Issue, 7, 75-119. 2007.

Pavlides, S. and Caputo, R.: Magnitude versus faults' surface parameters: quantitative relationships from the Aegean Region, Tectonophysics, 380,159–188, 2004.

Quidelleur, X., Gillot, P.Y., Grove, M., Harrison, T.M., Deino, A.: The White Trachytic Tuff Sanidine: a potential age standard
635 for 40Ar/39Ar dating of Pleistocene-Pliocene samples. Terra Cognita, pp. 69, 1997.

Roberts, G.P.: Variation in fault-slip directions along active and segmented normal fault systems, Journal of Structural Geology, 18, 835–845, 1996.

Roberts, G. P. and Michetti, A. M.: Spatial and temporal variations in growth rates along active normal fault systems: an example from The Lazio–Abruzzo Apennines, central Italy, Journal of Structural Geology, 26,339–376, 2004.

640 Rouchon, V., Gillot, P.Y., Quidelleur, X., Chiesa, S., and Floris, B.: Temporal evolution of the Roccamonfina volcanic complex (Pleistocene), Central Italy, Journal of Volcanology and Geothermal Research, 177, 500-514, https// doi.org/10.1016/j.jvolgeores.2008.07.016. 2008.

Rovida, A., Locati, M., Camassi, R., Lolli, B., and Gasperini, P.: The Italian earthquake catalogue CPTI15, Bulletin of Earthquake Engineering, 18, 2953-2984, https://doi.org/10.1007/s10518-020-00818-y, 2020.

645 Scarciglia, F., Mercatante, G., Fondevilla, V., Anadón, R., Oms, O., Donato, P., Agnini, C., Papini, M., Rook, L., and Ghinassi, M.: Pleistocene paleosol development and paleoenvironmental dynamics in East Africa: A multiproxy record from the Homo-bearing Aalat pedostratigraphic succession, Dandiero basin (Eritrea), Quaternary science reviews, 191, 275-298, 2018.

Schwertmann, U.: Differenzierung der Eisenoxide des Bodens durch photochemische Extraktion mit saurer Ammoniumoxalat-Lösung, Z. Pflanzenernahr. Dung. Bodenkd., 105, 194–202, 1964.

650 Stucchi, M., Meletti, C., Montaldo, V., Crowley, H., Calvi, G. M., and Boschi, E.: Seismic hazard assessment (2003-2009) for the Italian building code, Bulletin of the Seismological Society of America, 101, 1885–1911, https://doi.org/10.1785/0120100130, 2011.

Styron, R. and Pagani, M.: The GEM Global Active Faults Database, Earthquake Spectra, 36, 160–180, 2020.

Tangari, A.C., Scarciglia, F., Piluso, E., Marinangeli, L., and Pompilio, L.: Role of weathering of pillow basalt, pyroclastic 655 input and geomorphic processes on the genesis of the Monte Cerviero upland soils (Calabria, Italy), Catena, 171, 299–315, 2018

Valente, E., Buscher, J. T., Jourdan, F., Petrosino, P., Reddy, S. M., Tavani, S., Corradetti, A., and Ascione, A.: Constraining mountain front tectonic activity in extensional setting from geomorphology and Quaternary stratigraphy: A case study from the Matese ridge, southern Apennines, Quaternary Science Reviews, 219, 47-67, 660 https://doi.org/10.1016/j.quascirev.2019.07.001, 2019.

Valentini, A., Pace, B., Boncio, P., Visini, F., Pagliaroli, A., and Pergalani, F.: Definition of seismic input from fault-based PSHA: Remarks after the 2016 central Italy earthquake sequence, Tectonics, 38, 595–620, https://doi.org/10.1029/2018TC005086, 2019.

van Reeuwijk, L.P.: Procedures for soil analysis, in: Technical Paper,9, 6th ed., International Soil Reference and Information 665 Centre,119pp.,2002.

Wells, D.L. and Coppersmith, K.J.: New Empirical Relationships among Magnitude, Rupture Length, Rupture Width, Rupture Area, and Surface Displacement, Bulletin of the Seismological Society of America, 84, 974-1002, 1994.

Wesnousky, S.G.: Displacement and Geometrical Characteristics of Earthquake Surface Ruptures: Issues and Implications for Seismic-Hazard Analysis and the Process of Earthquake Rupture, Bulletin of the Seismological Society of America, 98, 1609–670 1632, https://doi.org/10.1785/0120070111, 2008.

Table 1. Summary of ^{40}Ar/^{39}Ar experiments

							Weighted mean
Sample	Material	N			MSWD		Age (ka) $\pm 2\sigma$
S228-F2	sanidine	12	of	19	0.94		508.5 $\pm$ 0.9
S277	sanidine	6	of	16	0.80		564.5 $\pm$ 2.1
C9-DO	sanidine	12	of	14	1.14		188.8 $\pm$ 3.0

Ages calculated relative to 1.1864 Ma Alder Creek sanidine (Jicha et al., 2016) using decay constants of Min et al. (2000)

Uncertainties shown at 95% confidence level

Table 2. Summary of radiocarbon datings

Site / geology	Sample	Material	Method – Lab.	Conventional Radiocarbon Age (BP)	Calendar Calibrated Results (95% prob.)
San Potito / Buried paleosol	S249-A	Charred material	AMS - Beta Analytic	38800 +/- 380 BP	41352 - 40260 cal BC (43301 - 42209 cal BP)
San Potito / colluvium	S227_5-1	Organic sediment	AMS - Beta Analytic	3000 +/- 30 BP	(89.4%) 1304 - 1126 cal BC (3253 - 3075 cal BP)
					(6.0%) 1377 - 1348 cal BC (3326 - 3297 cal BP)
San Potito / colluvium	S228_1ter	Charred material	AMS - Beta Analytic	370 +/- 30 BP	Cal AD 1445 to 1530 (Cal BP 505 to 420)
					Cal AD 1545 to 1635 (Cal BP 405 to 315)
San Potito / colluvium	S228_7-1	Organic sediment (bulk organic fraction)	AMS - Beta Analytic	104.71 +/- 0.39 pMC	(95.4%) post AD 1950
San Potito / buried paleosol	S228_3	Organic sediment (bulk organic fraction)	AMS - CEDAD	7561 ± 60	6510BC (95.4%) 6250BC
S. A. d'Alife / colluvium	C1_Donia_E	Organic sediment (bulk organic fraction)	AMS - Beta Analytic	1290 +/- 30 BP	Cal AD 660 to 770 (Cal BP 1290 to 1180)
S. A. d'Alife / colluvium	C3_Donia_E	Organic sediment (bulk organic fraction)	AMS - Beta Analytic	690 +/- 30 BP	Cal AD 1270 to 1305 (Cal BP 680 to 645) and Cal AD 1365 to 1385 (Cal BP 585 to 565)
S. A. d'Alife / colluvium	C7_Donia_W	Organic sediment (bulk organic fraction)	AMS - Beta Analytic	670 +/- 30 BP	Cal AD 1275 to 1315 (Cal BP 675 to 635) and Cal AD 1355 to 1390 (Cal BP 595 to 560)
S. A. d'Alife / colluvium	C8_Donia_W	Organic sediment (bulk organic fraction)	AMS - Beta Analytic	2703 +/- 30 BP	908 - 805 Cal BC (2855 - 2755 Cal BP)

675

Table 3

Measured throw and throw rates along the Gioia Sannitica (GF) and Ailano-Piedimonte Matese (APMF) normal faults

Code	Long	Lat	Fault	F. section	Site/Profile n.	throw (m)	method	Window (ka)	throw rate (mm/yr)	Source
GF1	14.3896	41.3526	GF	San Potito	Pr. 1	3	topog. prof.	15±3	0.21±0.04	this work
GF2	14.3973	41.3491	GF	San Potito	Pr. 2	6.5	topog. prof.	15±3	0.45±0.09	this work
GF3	14.3992	41.3478	GF	San Potito	Pr. 3	36	topog. prof.	<450 (post U1)	> 0.08	this work
GF4	14.3997	41.3470	GF	San Potito	Pr. 4	4	topog. prof.	10 (Holoc.)	0.40	this work
GF5	14.4034	41.3436	GF	San Potito	Pr. 5	7	topog. prof.	15±3	0.49±0.1	this work
GF7	14.4105	41.3406	GF	San Potito	Pr. 7	5	topog. prof.	15±3	0.35±0.07	this work
GF228	14.4182	41.3364	GF	San Potito	S.Potito site	>2.4	dated sedim.	≤8.145	>0.29	this work
GF9	14.4212	41.3338	GF	San Potito	Pr. 9	14.5	topog. prof.	<450 (post U1)	> 0.03	this work
GF10	14.4312	41.3254	GF	San Potito	Pr. 10	2.5	topog. prof.	15±3	0.17±0.03	this work
GF11	14.4544	41.3188	GF	M. Erbano embayment	Pr. 11	18	topog. prof.	<780 (post sd1)	> 0.02	this work
GF12	14.4529	41.3096	GF	Castello di Gioia	Pr. 12	85	topog. prof.	<780 (post sd1)	> 0.11	this work
GF13	14.4544	41.3022	GF	Castello di Gioia	Pr. 13	6.5	topog. prof.	15±3	0.45±0.09	this work
GF14	14.4572	41.2992	GF	Castello di Gioia	Pr. 14	7	topog. prof.	15±3	0.49±0.1	this work
GF15	14.4598	41.2961	GF	Castello di Gioia	Pr. 15	4	topog. prof.	15±3	0.28±0.06	this work
APMF1	14.2907	41.3532	APMF	Raviscanina	Section D	50-60	geologic section	<350	≥0.16	Boncio et al, 2016
APMF2	14.2271	41.3793	APMF	Raviscanina	Ps4	2±0.1	topog. prof.	15±3	0.14±0.03	Boncio et al, 2016
APMF3	14.2846	41.3537	APMF	Raviscanina	Ps5	2.9±0.6	topog. prof.	15±3	0.2±0.04	Boncio et al, 2016
APMF4	14.2864	41.3534	APMF	Raviscanina	S.Angelo d'Alife site	≥0.8	dated sedim.	≤2.285	>0.35	this work
APMF5	14.2982	41.3534	APMF	Raviscanina	Section F	65-105	geologic section	230-350	0.29±0.1	Boncio et al, 2016

680 **Table 4**

Magnitudes obtained from surface fault length and possible rupture scenarios for historical earthquakes

| Fault | Length (L) (km) | Magnitude | | | | | possible rupture scenarios (historical earthquakes) | |
		W&C94 NF	P&C04	W08 ALL	Gal08	average		
Gioia Sannitica (GF)	11.5	6.3	6.1	6.4	6.1	6.2	1293	1293 (M >>historical)
Ailano - Piedimonte Matese (APMF)	18.5	6.5	6.4	6.6	6.4	6.5	1349 (south prolong. AIF rupture?)	
Raviscanina section of APMF	11.5	6.3	6.1	6.4	6.1	6.2		
APMF + GF	30	6.8	6.7	6.8	6.7	6.8	346 (847?)	346 (847?)

W&C94 = Wells and Coppersmith, 1994 (Normal Faulting); P&C04 = Pavlides and Caputo, 2004; W08 ALL = Wesnousky, 2008 (ALL kinematics); Gal08 = Galli et al., 2008. AIF = Aquae Iuliae fault.

685
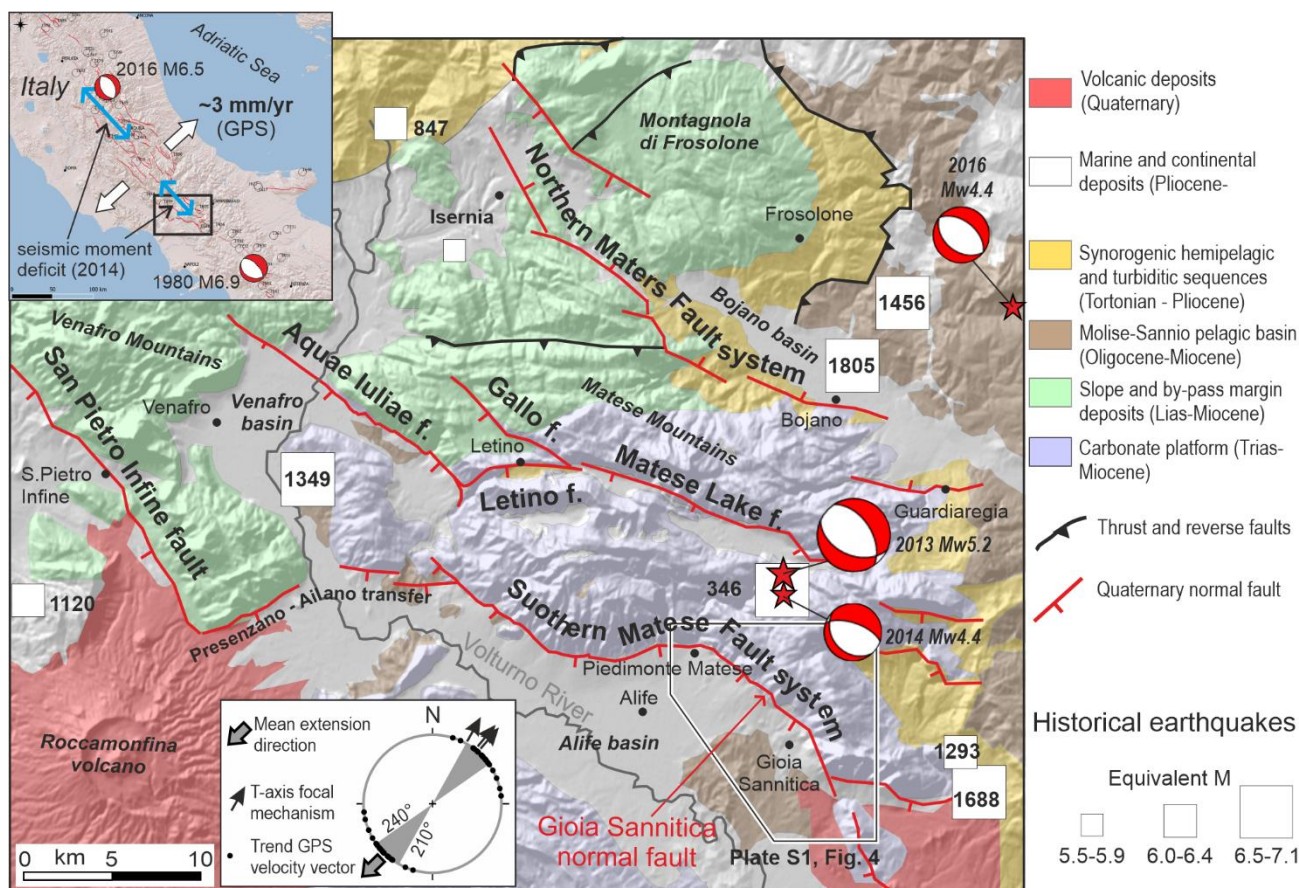
Figure 1: Simplified tectonic map of the Matese area (southern Apennines) with traces of Quaternary normal faults, epicentres of largest historical earthquakes (from CPTI15, Rovida et al., 2020) and locations of the Southern Matese Fault system and Gioia Sannitica normal fault studied in this work. Extensional directions are from Boncio et al. (2016). Focal mechanisms are from RCMT
690 **Catalogue (http://mednet.rm.ingv.it/rcmt.php). In location map: double arrows parallel to the Apennines indicate areas of seismic moment deficit (M≥6.5), compared to tectonic (geodetic) strain accumulated in the last 500 years, according to D'Agostino (2014); focal mechanisms refer to M≥6.5 instrumental earthquakes; circles are historical earthquakes with M≥6.0 (CPTI15).**
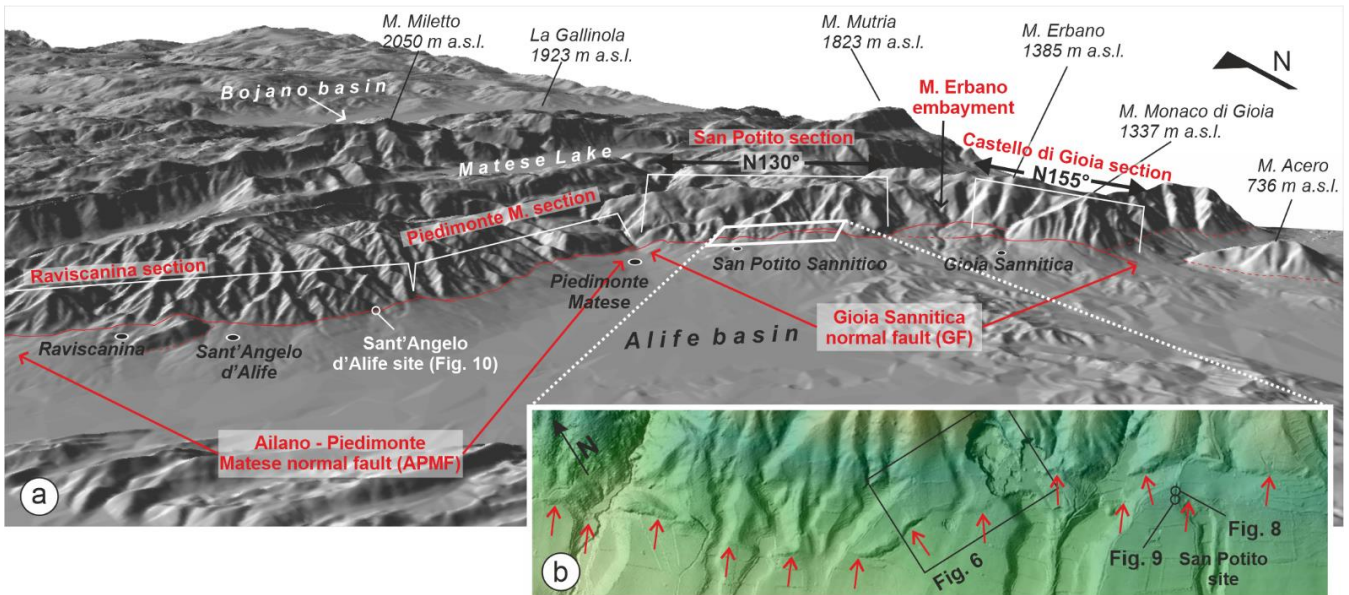
Figure 2: a) Oblique view of the southern Matese mountain front from a 5-m resolution Digital Elevation Model (DEM) with traces of the Ailano-Piedimonte Matese (APMF) and Gioia Sannitica (GF) normal faults, and b) detail of the GF fault trace, pointed by red arrows, on a 1-m resolution DEM from airborne Light Detection and Ranging (LiDaR).
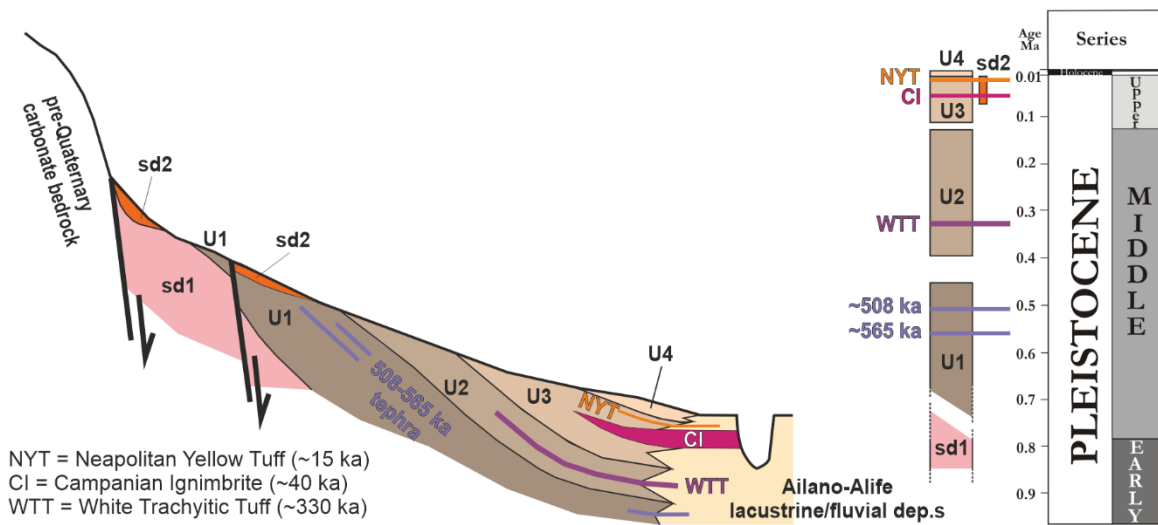
Figure 3: Morpho-stratigraphic relations and ages of Quaternary units in the southern Matese area.

Figure 4: Geologic map of the Gioia Sannitica normal fault (additional details and cross sections in Plate S1 of the supplementary material). In Section 1, C&R 99 = Corniello and Russo, 1999.

Figure 5: Field view of the Gioia Sannitica normal fault on carbonate bedrock (a, b, c; San Potito fault section) and on Quaternary breccia (c; Castello di Gioia fault section). Location in Fig. 4.

Figure 6: Geologic detail and topographic profiles across the Gioia Sannitica normal fault trace (San Potito fault section). The topography is from the 1-m resolution LiDaR DEM. Location in Fig.s 2b and 4.
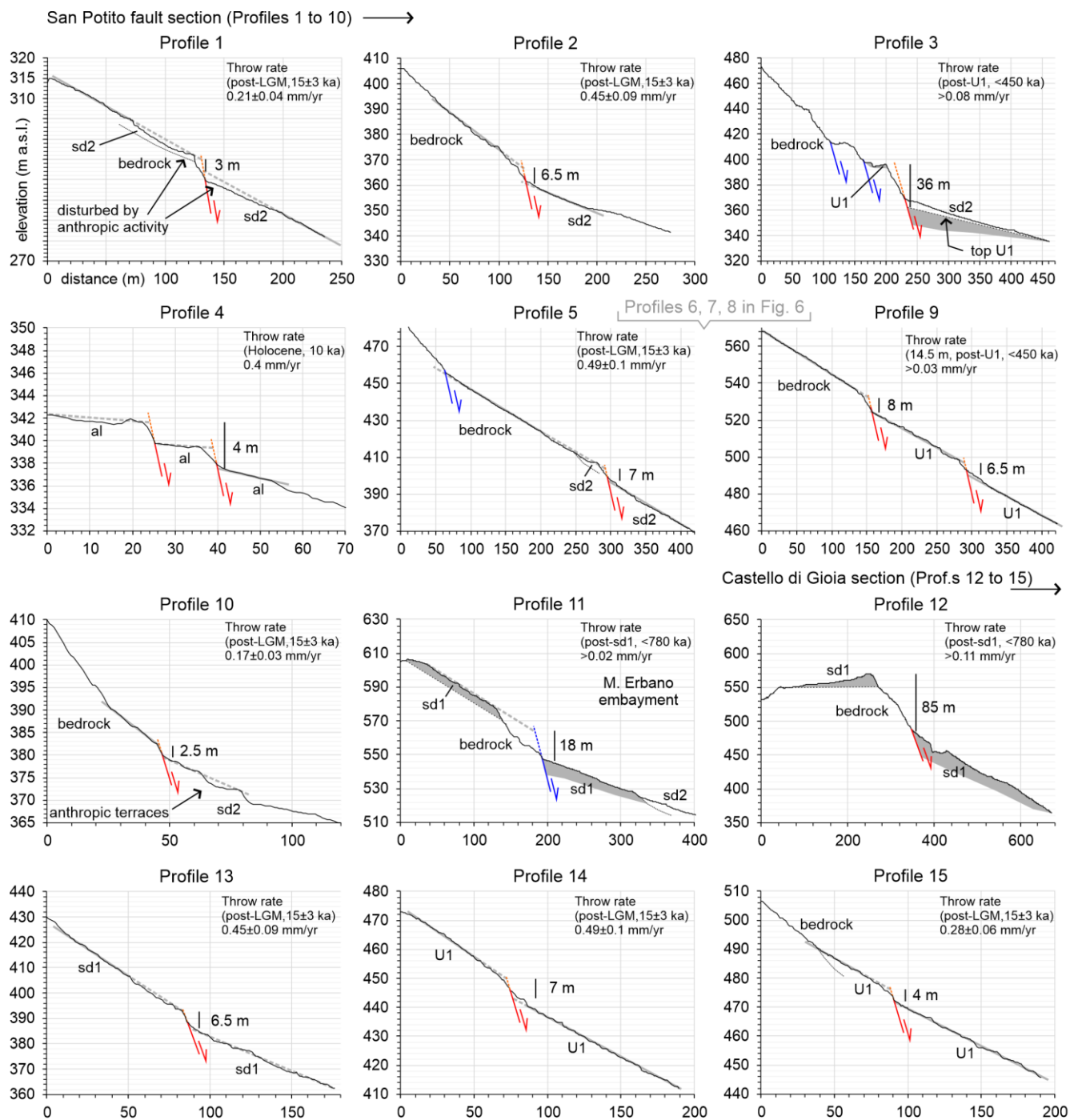
Figure 7: Topographic profiles across the Gioia Sannitica normal fault trace extracted from the 1-m resolution LiDaR DEM and estimated throw rates (see also Tab. 3). Location of profile traces in Fig. 4.
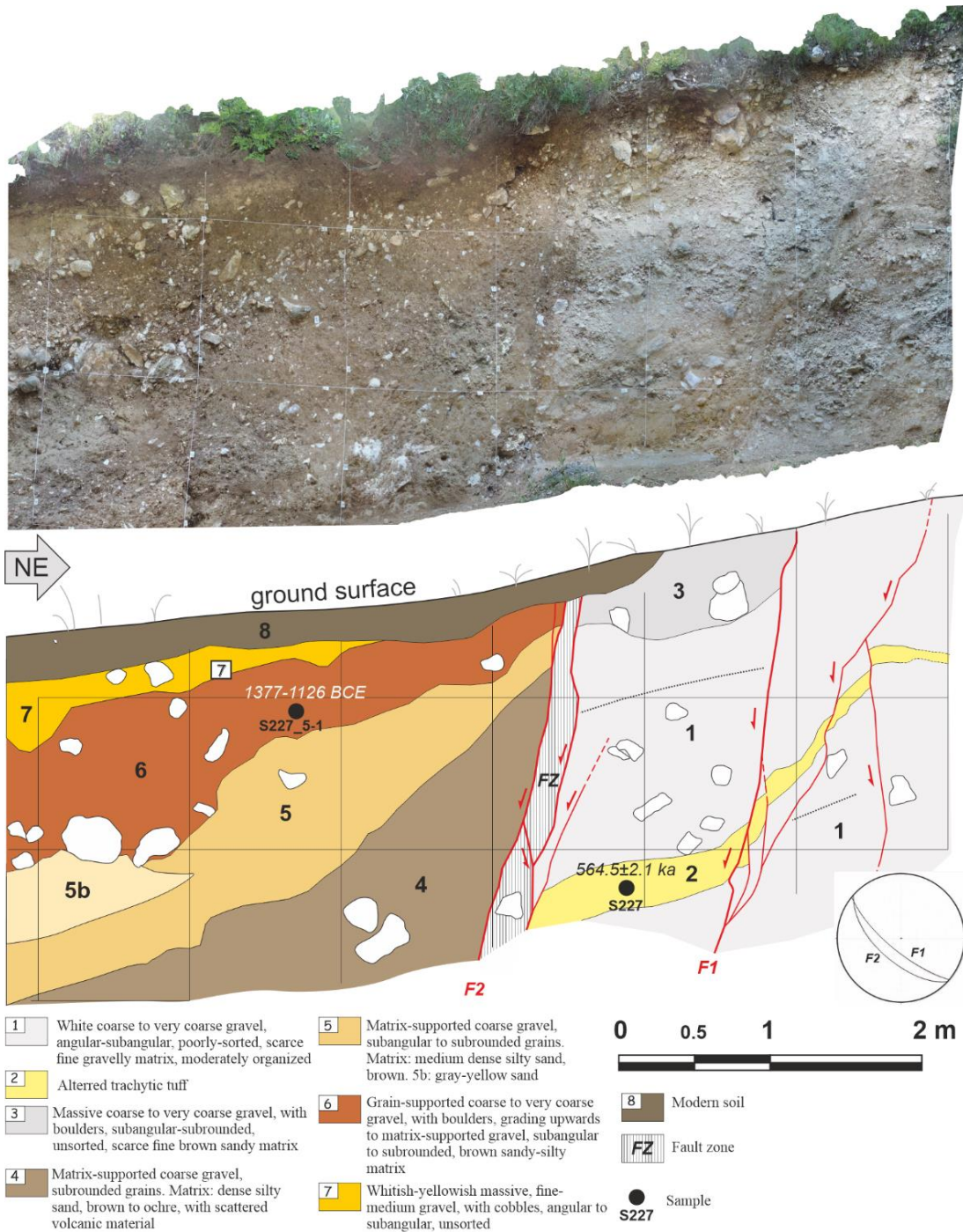
Figure 8: Photomosaic and interpreted log of fault zone 1 in the western splay of the Gioia Sannitica normal fault (San Potito fault section, central part). Complete details of age determinations in Tab.s 1 and 2 and in Tab. S1 of the supplementary material. Location in Fig.s 2b and 4.
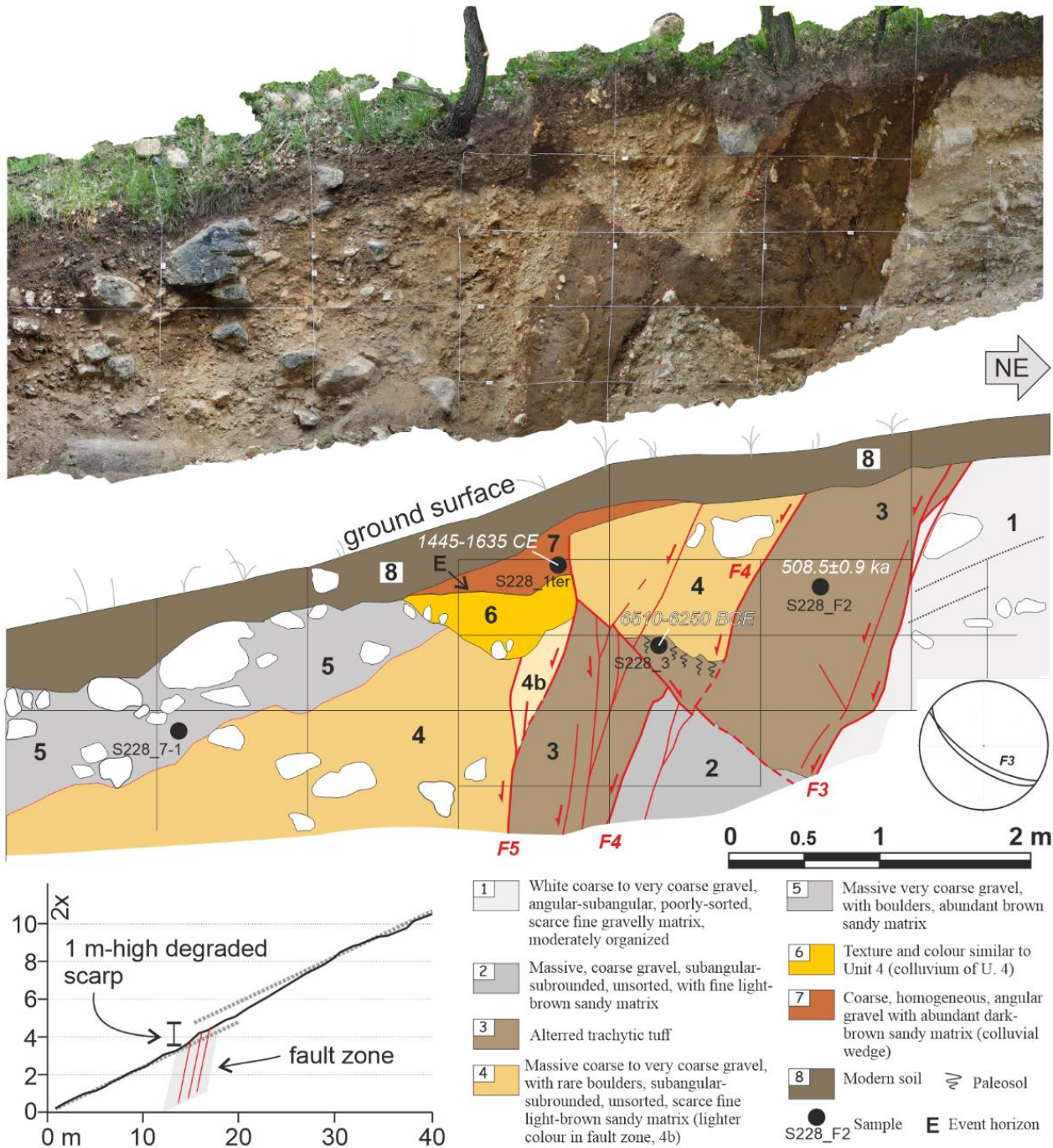
Figure 9: Photomosaic and interpreted log of fault zone 2 and micro-topographic profile across the fault zone in the western splay
of the Gioia Sannitica normal fault (San Potito fault section, central part). Event horizon (E) = topographic surface at the time of
the last surface faulting event. Complete details of age determinations in Tab.s 1 and 2 and in Tab. S1 of the supplementary material.
Detailed analysis of the paleosol (sample S228_3) in Text S1 of the supplementary material. Location in Fig.s 2b and 4.
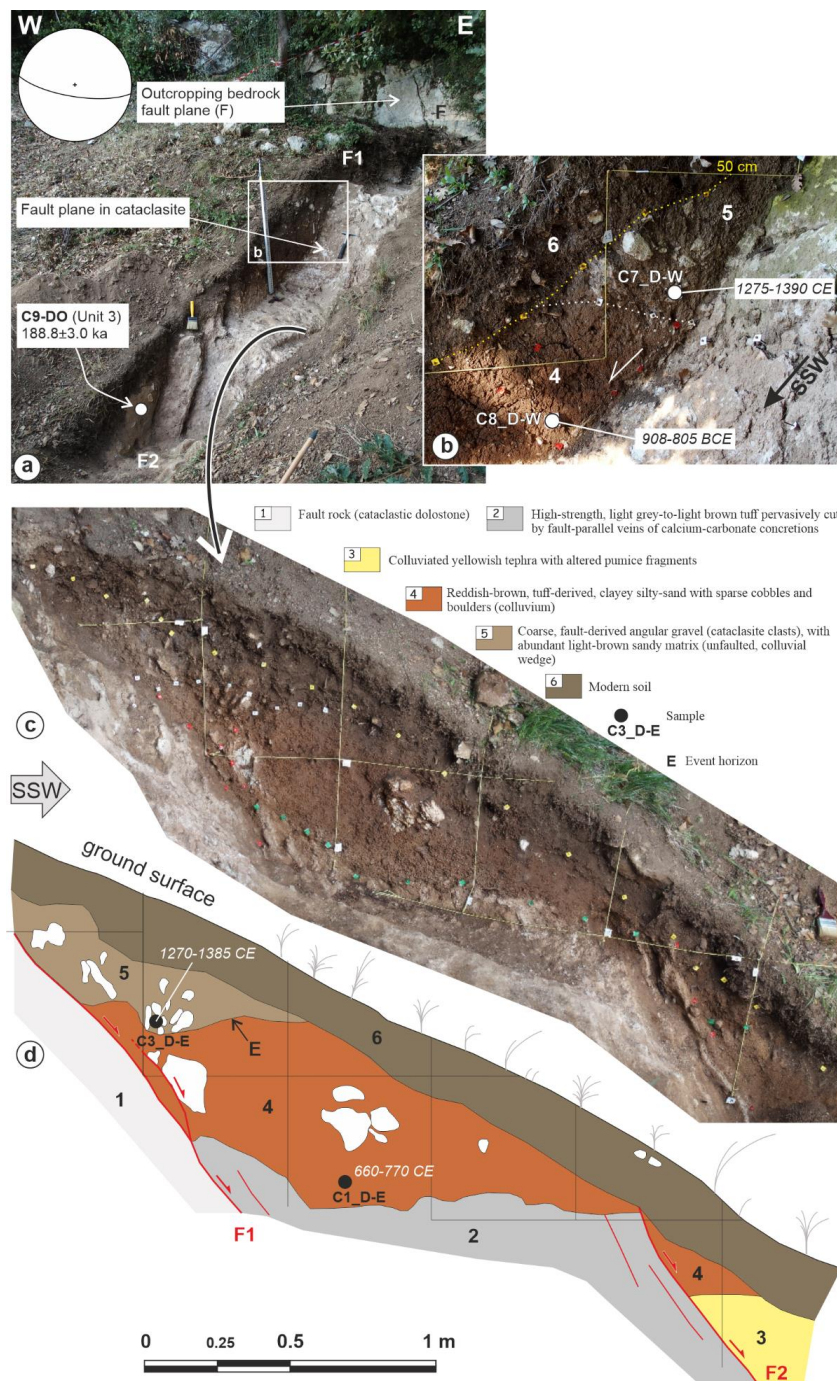
730 **Figure 10: Field view to the North (a), detail (b), and photomosaic and log of the southern wall (c, d) of a shallow hand-dug trench across the southern Ailano-Piedimonte Matese fault (Raviscanina fault section, southern part) near Sant'Angelo d'Alife. Event horizon (E) = topographic surface at the time of the last surface faulting event. Complete details of age determinations in Tab.s 1 and 2 and in Tab. S1 of the supplementary material. Location in Fig. 2a.**
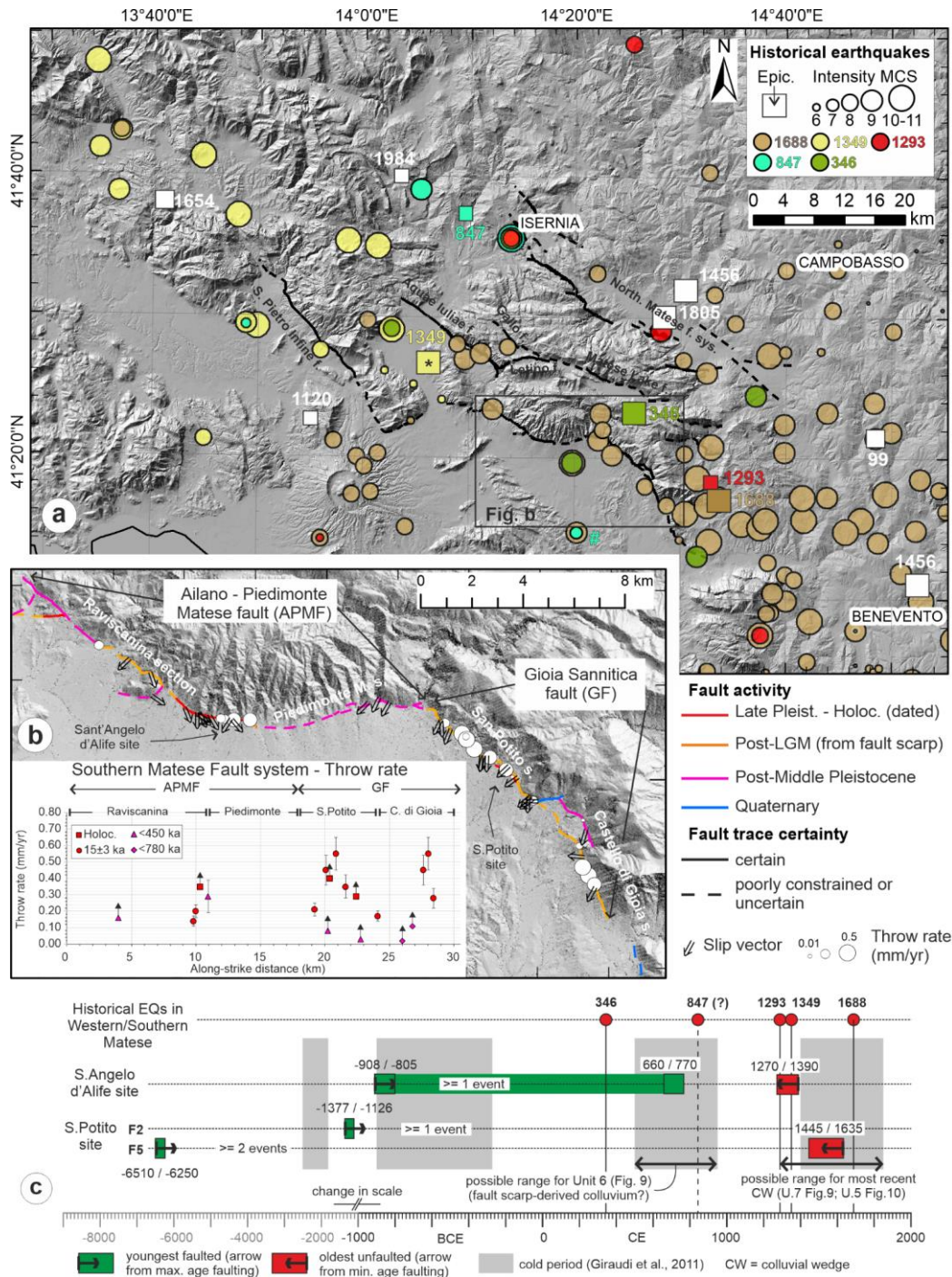
Figure 11: a) Distribution of intensity data points (from DBMI15, Locati et al., 2021) of the largest historical earthquakes in the Matese area (* = epicentre from Galli and Naso, 2009; # = intensity data point from Bottari et al., 2020). **b)** Fault activity classification and along-strike throw rate distribution of the Southern Matese Fault system. **c)** Age constraints for surface faulting events according to data collected in the San Potito (GF) and Sant'Angelo d'Alife (APMF) sites compared with the ages of historical earthquakes.
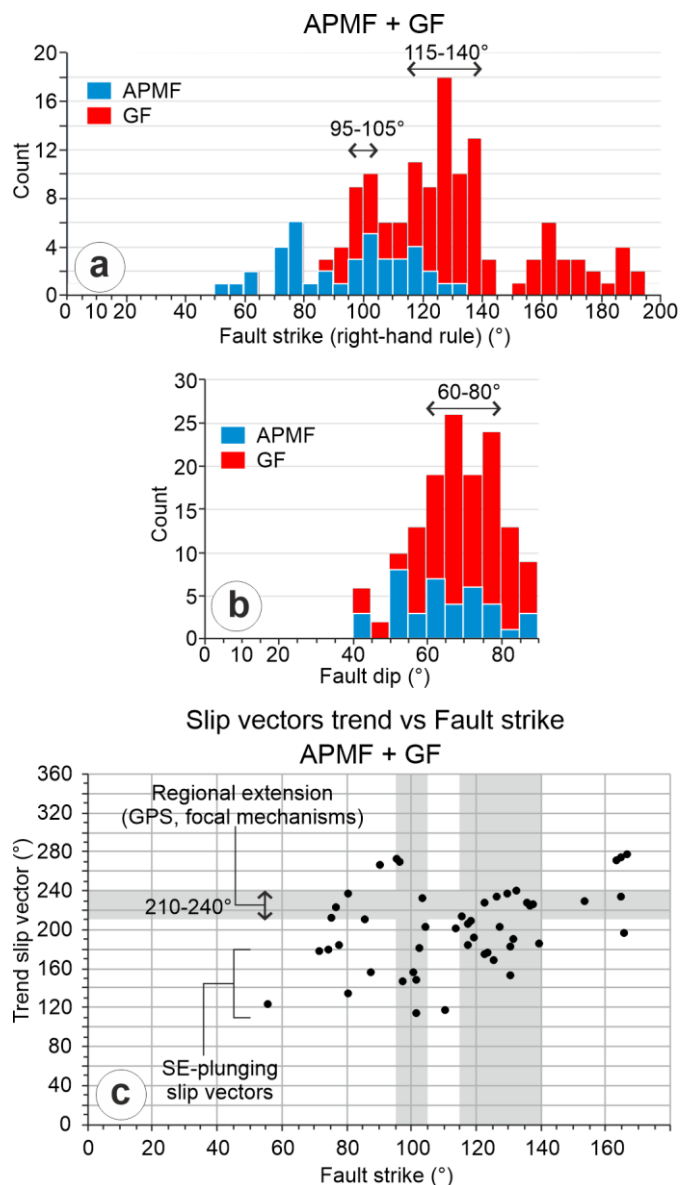
Figure 12: Summary of structural data for fault strike (a), fault dip (b) and slip vector trend (d) collected along the Southern Matese Fault system in this work (GF) and in Boncio et al. 2016 (APMF). Grey vertical bands in (c) correspond to the ranges of strike most represented in (b).

745